RESEARCH ARTICLE

The receptor-like kinase BIR1 inhibits elicitor-induced plasmodesmata callose deposition and PTI gene expression and requires EDS1 and SOBIR1 to cause dose-dependent cell-death in Arabidopsis

Irene Guzmán-Benito[1], Carmen Robinson[1], Chenlei Hua[2], Ana Rocio Sede[3], Laura Elvira-González[3], Isabel Punzón[1], Manfred Heinlein[3], Thorsten Nürnberger[2,4], César Llave[1]*

[1]Centro de Investigaciones Biológicas Margarita Salas. Consejo Superior de Investigaciones Científicas, Ramiro de Maeztu 9, 28040 Madrid, Spain; [2]Department of Plant Biochemistry, Center of Plant Molecular Biology (ZMBP), University of Tübingen, Tübingen, Germany; [3]Institut de Biologie Moléculaire des Plantes, CNRS, Université de Strasbourg, 67000 Strasbourg, France; [4]Department of Biochemistry, University of Johannesburg, Johannesburg, South Africa.

Author for correspondence: César Llave

E-mail: cesarllave@cib.csic.es

Phone: +34-91-8373112

Summary

- The receptor-like kinase BIR1 functions as a negative regulator of cell death and defense in Arabidopsis. Previous studies showed that BIR1 expression is up-regulated during infections with microbes and viruses. However, the biological consequences of BIR1 induction remain unknown.
- Here, we use a DEX-inducible expression system in Arabidopsis to investigate the outputs associated with physiological and non-physiological levels of BIR1 expression.
- We show that BIR1 induction at physiological levels significantly interferes with gene expression and plasmodesmata callose deposition triggered by canonical PTI elicitors. We found that plants that accumulated non-physiological doses of BIR1 displayed morphological defects that concur with transcriptomic changes in multiple plant defense genes. We provide experimental evidence that EDS1 and SOBIR1 are required for the ETI-type cell death phenotypes associated to non-physiological levels of BIR1
- Here we propose that BIR1 induction may represent a pathogen-triggered mechanism to modulate plant defenses during infection. Our model predicts that when BIR1 regulation is lost, BIR1 integrity is sensed by one or several guarding resistance (R) proteins to initiate an ETI-like response, in which SOBIR1 cooperates with EDS1 to transduce signals downstream of R proteins.

Key words

Arabidopsis, immune regulation, immune receptor, cell death, BAK1-INTERACTING RECEPTOR-LIKE KINASE 1 (BIR1), SUPPRESSOR OF BIR1 (SOBIR1), ENHANCED DISEASE SUSCEPTIBILITY 1 (EDS1)

Introduction

Plants use immunity to defend themselves against invaders such as bacteria, fungi, oomycetes, and viruses (Korner *et al.*, 2013; Macho & Lozano-Duran, 2019; Nishad *et al.*, 2020; Ngou *et al.*, 2022). This system involves multiple cell-surface pattern recognition receptors (PRR) that recognize pathogen/microbe/damage-associated molecular patterns (PAMP/MAMP/DAMP), leading to pattern-triggered immunity (PTI), and intracellular receptors that sense pathogen-effector proteins or effector-induced manipulations of host proteins, leading to effector-triggered immunity (ETI) (Li *et al.*, 2020; Zhou & Zhang, 2020; Lee *et al.*, 2021; Yu *et al.*, 2021). PRRs are single-transmembrane receptor-like kinases (RLK) or receptor-like proteins (RLP), which form active receptor complexes in a ligand-dependent manner with members of the somatic embryogenesis co-receptor kinases (SERKs), including BRASSINOSTEROID INSENSITIVE1-ASSOCIATED RECEPTOR KINASE 1 (BAK1/SERK3) (Boutrot & Zipfel, 2017; Hohmann *et al.*, 2017; Tang *et al.*, 2017; Smakowska-Luzan *et al.*, 2018; Lee *et al.*, 2021). BAK1 functions as a positive regulator of PTI (Liebrand *et al.*, 2014; Wu *et al.*, 2020), and has a dual role as positive and negative regulator of cell death during ETI (Belkhadir *et al.*, 2012; Dominguez-Ferreras *et al.*, 2015). RLP-type PRRs lack kinase activity and constitutively associate in a ligand-independent manner with the leucine-rich repeat (LRR)-RLK adapter SUPPRESSOR OF BIR1-1 (SOBIR1) (Gust *et al.*, 2017). Once the microbe is sensed, PRR receptor complexes activate, via trans-phosphorylation, receptor-like cytoplasmic kinases (RLCKs) that initiate downstream signaling cascades (Tang *et al.*, 2017; Liang & Zhou, 2018; Rao *et al.*, 2018). Among them, BOTRYTIS INDUCED KINASE1 (BIK1) functions either as a positive regulator of immunity triggered by LRR-RLKs such as those induced by the flg22 peptide derived from bacterial flagellin (FLAGELLIN SENSING 2, FLS2), or as a negative regulator of immunity triggered by LRR-RLPs such as those induced by the nlp20 fragment of NECROSIS AND ETHYLENE-INDUCING PEPTIDE 1 (NEP1)-LIKE proteins (NLP, RLP23) (Bi *et al.*, 2018; Wan *et al.*, 2019).

ETI relies on nucleotide-binding domain LRR intracellular immune receptors (NLRs) encoded by polymorphic disease resistance genes (R). NLRs comprise either proteins with an N-terminal domain similar to the TOLL/INTERLEUKIN RECEPTOR 1 (TIR1) (TIR-NB-LRR, TNL), proteins with a coiled-coil (CC) domain at the N terminus (CC-NB-LRR, CNL) or proteins with a RESISTANCE TO POWDERY MILDEW 8-LIKE DOMAIN (RPW8)-type domain (RNLs) (McHale *et al.*, 2006; van Wersch *et al.*, 2020; Wang & Chai, 2020). NLRs function as "sensors" that recognize effectors, or as "helpers" that act downstream of sensor NLRs in ETI

signaling (Jubic *et al.*, 2019). Recent studies demonstrated that PTI and ETI work together to mutually potentiate the immune response (Yuan *et al.*, 2021b; Yuan *et al.*, 2023). For instance, NLR-mediated signaling is dependent on multiple PTI-associated components such as BAK1, SOBIR1, or BIK1 in a PTI-independent manner, while TNL genes that are up-regulated during early PTI boost immune responses (Ngou *et al.*, 2021; Tian *et al.*, 2021; Yuan *et al.*, 2021a). ENHANCED DISEASE SUSCEPTIBILITY (EDS1), which is essential in TNL-mediated immunity, also plays a key role in PTI signaling in response to different microbial elicitors (Pruitt *et al.*, 2021b; Tian *et al.*, 2021). Furthermore, PTI and ETI outputs usually converge, albeit with different amplitude and duration (Yuan *et al.*, 2021b). Early responses include apoplastic reactive oxygen species (ROS) burst, cytosolic calcium (Ca^{+2}) influx and activation of Ca^{+2}-dependent protein kinases (CPK), and activation of mitogen-activated protein kinases (MAPK). This response is followed by the transcriptional activation of defense processes that include accumulation of defense phytohormones, regulation of cell wall and secretome composition, and cellular motion (Li *et al.*, 2020).

Plants deploy a variety of mechanisms to protect themselves from the detrimental effects of hyperactivated defenses (Couto & Zipfel, 2016; Withers & Dong, 2017; Mithoe & Menke, 2018). BAK1-INTERACTING RECEPTOR-LIKE KINASE (BIR) proteins play a key role in defense attenuation. The current model postulates that, in the absence of microbes, BIR proteins constitutively associate with BAK1, thus maintaining the PRRs in a resting state. During ligand perception, BAK1 dissociates from BIR and becomes accessible to complex with PRR receptors (Gao *et al.*, 2009; Halter *et al.*, 2014; Imkampe *et al.*, 2017). The Arabidopsis genome has four BIR homologs (Halter *et al.*, 2014). BIR1 exerts a tight control of BAK1- and SOBIR1-mediated cell death signaling, presumably related to PRR-RLP-ligand perception (Albert *et al.*, 2015; Liu *et al.*, 2016). BIR2 and BIR3 have critical roles in the negative regulation of PRR-mediated PTI (Halter *et al.*, 2014; Imkampe *et al.*, 2017). Unlike BIR2 and BIR3, BIR1 possesses phosphorylation activities (Gao *et al.*, 2009). Interestingly, knocking-out BIR1 triggers resistance pathways that implicate components of TNL-mediated ETI response, suggesting that loss of BIR1 activates one or several unknown TNL proteins (Gao *et al.*, 2009; Liu *et al.*, 2016; Schulze *et al.*, 2022).

BIR1 expression is transcriptionally activated in response to multiple microbial and viral pathogens in a salicylic acid (SA)-dependent manner (Guzman-Benito *et al.*, 2019). To date, the effects of BIR1 induction on the outcome of plant defenses remain largely unknown. However, previous work showed that transgenic overexpression of BIR1 triggers

112 developmental defects and cell death similar to the autoimmune phenotypes observed in *bir1-*
113 *1* mutants (Gao *et al.*, 2009; Guzman-Benito *et al.*, 2019). Although the consequences of BIR1
114 overexpression have not been fully characterized yet, this finding seems to indicate that
115 perturbations in BIR1 homeostasis have severe growth-defense penalties. Clearly, effective
116 strategies for BIR1 regulation are needed to prevent unbearably high levels of BIR1 expression.
117 In this regard, RNA-directed DNA methylation and post-transcriptional RNA silencing regulate
118 levels of BIR1 transcripts when BIR1 is actively transcribed (Guzman-Benito *et al.*, 2019).

119 In this work, we conducted a time-course analysis to investigate the phenotypical outputs
120 associated with physiological and non-physiological levels of BIR1 expression in Arabidopsis
121 plants. We show that physiological induction of BIR1 interferes with the expression of PTI
122 marker genes and plasmodesmata (PD)-associated callose deposition in response to several PTI
123 elicitors, but not with ethylene accumulation or ROS production. Whereas physiological
124 induction of BIR1 has a subtle impact on the plant transcriptome, the morphological and growth
125 defects caused by the sustained expression of BIR1 are concomitant with the transcriptional
126 reprogramming of multiple genes encoding components of PTI and ETI signaling pathways.
127 We found that the cell death phenotypes associated with prolonged BIR1 overexpression
128 require the TNL-associated EDS1 and/or the RLP-co-receptor SOBIR1, but the underlying
129 mechanism is unknown. Finally, our work demonstrates that a well-balanced expression of
130 BIR1 avoids interference with cellular processes of growth and development, and is critical for
131 plant fitness.

132

133 **Material and methods**

134 **Plant material and growth condition**

135 *Arabidopsis thaliana* plants were grown in controlled environmental chambers under long-day
136 conditions (16h day/8h night) at 22°C. Arabidopsis lines used in this study were derived from
137 the Columbia-0 (Col-0) ecotype. Seeds were surface-sterilized and sown on plates containing
138 ½ Murashige and Skoog (MS) medium supplemented with MES (0,5g/L), 1% sucrose and 0,9%
139 Plant agar (Duchefa Biochemie). Seedlings were transferred to soil seven to ten days after
140 germination.

141 Mutants for *bir1-1* and *sobir1-12* were donated by Yuelin Zhang (University of British
142 Columbia, Canada). The Arabidopsis *eds1-2*, *pad4-1* and *eds5-3* alleles were supplied by Jane
143 E. Parker (Max Planck Institute for Plant Breeding Research, Germany). Arabidopsis mutant

144 *bak1-5* was donated by Birgit Kemmerling (Center of Plant Molecular Biology, University of
145 Tübingen, Germany). The *sid2-2* mutant was a gift from Francisco Tenllado (Centro de
146 Investigaciones Biológicas Margarita Salas, CSIC, Spain).

147 Arabidopsis Col-0 transgenic plants expressing a BIR1-mCherry fusion under a dexamethasone
148 (DEX)-inducible gene expression system (BIR1 L6 and BIR1 L9) have already been described
149 (Guzman-Benito *et al.*, 2019). In this study, the same DEX-inducible expression system
150 containing a mCherry-tagged BIR1 (herein BIR1) protein-coding gene was transformed into
151 Arabidopsis mutant backgrounds according to standard floral dipping (Clough & Bent, 1998).
152 Independent homozygous lines were selected in T3 and used for subsequent experiments.
153 Unless otherwise indicated, morphological phenotypes after DEX treatments were investigated
154 in two independent transgenic lines of each genotype.

155 **RNA analysis**

156 Total RNA was extracted using TRIzol reagent (Invitrogen) and treated with DNase I
157 (Invitrogen) following manufacturer's instructions to eliminate genomic DNA traces. One-step
158 quantitative RT-PCR (RT-qPCR) was carried out using Brilliant III Ultra-Fast SYBR Green
159 QRT-PCR Master Mix (Agilent Technologies) in a Rotor-Gene 6000/Rotor-Gene Q real-time
160 PCR machine (Corbett/Qiagen) (Fernandez-Calvino *et al.*, 2016). Relative gene expression was
161 determined using the Delta-delta cycle threshold method and Rotor-Gene 6000 Series Software
162 (Corbett). Transcript levels of the target genes were normalized to the transcript levels of the
163 housekeeping gene *CBP20* (*At5g44200*) as a reference gene. Primers are listed in Table S1.

164 **Protein analysis**

165 Leaf tissue samples were ground in liquid nitrogen in an Eppendorf tube and homogenized in
166 extraction buffer (65 mM Tris-HCl, pH 8; 3% sodium dodecyl sulfate [SDS]; 1% ß-
167 mercaptoethanol; 10% glycerol). Samples were diluted in Laemmli buffer, incubated for 5 min
168 at 95°C, and loaded onto 10% SDS-PAGE protein gels. After electrophoresis, proteins were
169 blotted onto an ECL nitrocellulose membrane (Amersham-Pharmacia), and detected using
170 commercial horseradish peroxide (HRP)-conjugated secondary antibodies and a
171 chemiluminescent substrate (LiteAblot Plus). Primary and secondary antibodies were diluted
172 according to the manufacturer's recommendations. The RFP-Trap (Chromotek) was used for
173 immunoprecipitation of mCherry-tagged BIR1 protein from Arabidopsis leaves following
174 manufacturer's instruction.

175 **RNA and library preparation for transcriptome sequencing**

176 Total RNA was extracted from each sample using the RNeasy plant mini kit (Qiagen) followed
177 by DNase treatment according to manufacturer's instructions. A total of 24 samples, including
178 three biological replicates per treatment, were collected. Each sample consisted of RNA pooled
179 from six individual plants. RNA degradation and contamination were monitored on 1% agarose
180 gels, and BIR1 transcript accumulation was measured by RT-qPCR. The RNA purity and RNA
181 concentration were checked using a Nanodrop spectrophotometer (ThermoFisher Scientific),
182 while the RNA integrity was measured using the Agilent Bioanalyzer 2100 system (Agilent
183 Technologies). Sequencing libraries were generated at NOVOGENE (HK) COMPANY
184 LIMITED (Wan Chai, Hong Kong) (www.novogene.com) using NEBNext® UltraTM RNA
185 Library Prep Kit for Illumina® (New England Biolabs) following manufacturer's
186 recommendations and index codes were added to attribute sequences to each sample. First-
187 strand cDNA from mRNA was synthesized using random hexamer primer and M-MuLV
188 Reverse Transcriptase (RNase H-). Second-strand cDNA synthesis was subsequently
189 performed using DNA Polymerase I and RNase H. NEBNext Adaptors with hairpin loop
190 structure were ligated. In order to select cDNA fragments of preferentially 150~200 bp in
191 length, the library fragments were purified with the AMPure XP system (Beckman Coulter).
192 PCR was done with Phusion High-Fidelity DNA polymerase, Universal PCR primers and Index
193 (X) Primer. PCR products were purified with the AMPure XP system and library quality was
194 assessed on the Agilent Bioanalyzer 2100 system. Clustering of the index-coded samples was
195 performed on a cBot Cluster Generation System using the TruSeq PE Cluster Kit v3-cBot-HS
196 (Illumina) according to the manufacturer's recommendations. Finally, paired-end reads were
197 generated via an Illumina PE150 Hiseq platform at NOVOGENE (HK) COMPANY LIMITED.

198 **Bioinformatics analysis of RNA-Seq data**

199 Clean reads were obtained by removing adaptor tags and reads containing poly-N and low-
200 quality reads from raw data. Paired-end clean reads were mapped to the Arabidopsis TAIR v10
201 reference genome using HISAT2 software. To quantify the gene expression levels, HTSeq
202 v0.6.1 was used to calculate the number of mapped reads of each gene and then normalize the
203 results to the expected number of Fragments Per Kilobase of transcript sequence per Millions
204 of base-pairs sequenced (FPKM). Differential expression analysis between groups (three
205 biological replicates per condition) was performed using DESeq2 R package (1.18.0). The
206 resulting *p-value*s were adjusted using the Benjamini and Hochberg's approach for controlling
207 the False Discovery Rate (FDR). Genes with an adjusted *p-value* ≤ 0.05 found by DESeq2 were
208 deemed as differentially expressed (DEG). Functional classification of DEGs including Gene

209 Ontology (GO) and KEGG was performed. GO enrichment analysis of DEGs was implemented
210 by tGOseq R package, in which gene length bias was corrected. KOBAS software was used to
211 test the statistical enrichment of DEGs in the KEGG database GO terms and KEGG pathways
212 with corrected *p-value* ≤0.05 were considered significantly enriched by DEGs. The raw data
213 was deposited in the Gene Expression Omnibus under accession number GSE234036.

214 **Reactive oxygen species (ROS) and ethylene measurement**

215 The detection of ROS and ethylene was performed as described (Albert *et al.*, 2015; Wan *et al.*,
216 2019). Approximately 4-wk-old BIR1 L9 or WT Arabidopsis plants were treated with 30 μM
217 DEX (H_2O was used as control) for 4 days at 24 h intervals and leaves were then cut into pieces
218 and left floating on H_2O overnight before measurement. For ROS assays, leaf pieces were
219 analyzed in a 96-well plate containing 20 μM L-012 (Wako Pure Chemical Industries Ltd) and
220 2 μg ml^{-1} peroxidase. Luminescence was measured both before (background) and over 1 h
221 following flg22 (GenScript Biotech) elicitation or mock treatment using a Mithras LB 940
222 luminometer (Berthold Technologies). For ethylene measurement, leaf pieces were incubated
223 in 20 mM MES buffer, pH 5.6 and the indicated elicitor (GenScript Biotech). Ethylene
224 accumulation was measured by gas chromatographic analysis (GC-14A) of 1 ml of the air
225 drawn from the closed tube with a syringe after the indicated incubation time. At least three
226 replicates were performed for all treatments.

227 **Callose staining**

228 Callose staining was carried out as described (Huang *et al.*, 2022; Huang *et al.*, 2023). Briefly,
229 approximately 4-wk-old BIR1 L9 or WT Arabidopsis plants were sprayed with 30 μM DEX
230 (H_2O was used as control) for 4 days at 24 h intervals and then leaf disks were excised and left
231 floating on H_2O. For callose staining, individual leaf disks were soaked with 0,1% aniline blue
232 solution (in 50 mM potassium phosphate buffer, pH 8.0) containing either 0.5 μg μl^{-1} poly(I:C)
233 (Sigma) or 1 μM flg22 (GenScript Biotech). Leaf disks were further evacuated for 1-2 minutes
234 (< 0.8 pa) in a vacuum desiccator. Aniline blue fluorescence was imaged 30 minutes after
235 poly(I:C)/flg22 or control treatment using a Zeiss LSM 780 confocal laser scanning microscope
236 with ZEN 2.3 software (Carl Zeiss) and using a 405 nm diode laser for excitation and filtering
237 the emission at 475-525 nm. mCherry fluorescence was excited at 561 nm filtering the emission
238 at 560-610 nm. 8-bit images were acquired with a Plant-Apochromat 40x/1.4 Oil DIC M27
239 objective. Callose fluorescence intensity was quantified with ImageJ software
240 (http://rsbweb.nih. gov/ij/) using the plug-in calloseQuant (Huang *et al.*, 2022). Callose spots

241 were measured in 3-4 images taken from each leaf disk. If not otherwise mentioned, three leaf
242 discs per plant from three different plants were evaluated for each genotype or condition.
243 Regions of interest (ROIs) selected by calloseQuant were verified visually before measurement.
244 Individual fluorescence intensities that occurred as outliers from the general distribution of
245 fluorescence intensities (<1%) in the sample were excluded from analysis.

246

247 **Results**

248 **BIR1 induction causes dose-dependent transcriptome reprogramming in Arabidopsis**

249 To understand the downstream biological processes and pathways associated with BIR1
250 induction, we conducted a global transcriptome RNA-Seq assay in Arabidopsis WT and BIR1
251 L9 plants that express a DEX-inducible BIR1-mCherry transgene (Guzman-Benito *et al.*,
252 2019). This system proved to be a valuable tool for studying the phenotypic outcomes caused
253 by different levels of BIR1 expression in the absence of pathogen elicitors or effectors. Three-
254 week-old plants were sprayed with a 30 µM DEX solution at 24 h intervals and rosette leaf
255 samples were harvested for next-generation sequencing. Control plants were mock-treated with
256 H_2O. Three biological replicates were used as representative samples for each condition tested
257 in this study: DEX-treated WT (DeWT_), mock-treated WT (MoWT_), DEX-treated BIR1 L9
258 (DeL9_) and mock-treated BIR1 L9 (MoL9_) plants at 4 or 12 days of treatment as indicated
259 **(Table S2)**. We found that BIR1 was induced at physiological levels in DeL9_ samples after 4
260 days of DEX treatment, and plants displayed WT morphologies **(Fig. 1A)**. In contrast, DeL9_
261 plants accumulated high doses of BIR1 (non-physiological), and exhibited a range of growth
262 defects and premature senescence after long BIR1 induction times (12 days of DEX treatment)
263 **(Fig. 1A)** (Guzman-Benito *et al.*, 2019). Principal component analysis (PCA) was used to sort
264 RNA-seq-based transcriptomic data according to gene expression levels. To discard the
265 potential effects of DEX on gene expression, we first compared DEX-treated WT versus DEX-
266 treated BIR1 L9 plants. PC1 defined a distinct separation in the PCA score plot between WT
267 (DeWT_12) and BIR1 L9 (DeL9_12) samples after 12 days of treatment, indicating that the
268 BIR1 expression level was the main source of variance (36.92%) **(Fig. 1B)**. Samples in the
269 DeL9_4 group, which produced physiological levels of BIR1 after 4 days of treatment,
270 clustered in the proximity of non-transgenic DeWT_4 samples, reflecting their similar
271 expression profiles. PC2 seems to highlight a shift in gene expression between samples due to
272 age or developmental stage (22.07%). When DEX-treated BIR1 L9 plants were compared with

273 mock-treated BIR1 L9 plants, the BIR1 expression level was again the dominant source of
274 variance (36.85%) underlying PC1, whereas time was the basis for PC2 (19.57%) separation in
275 the PCA score plot **(Fig. S1A).**

276 We noticed that normalized BIR1 abundance (FPKM) after 12 days of DEX treatment differed
277 between independent BIR1 L9 replicates (DeL9_12), perhaps due to the differences in DEX
278 sensitivity (**Fig. 1A**). The DeL9_12b sample within the DeL9_12 group was located far from
279 the other DeL9_12 samples in the PCA plot, and positioned near the samples within the
280 DeWT_12 or MoL9_12 clusters **(Figs. 1B, S1A)**. Noticeably, DeL9_12b produced fewer BIR1-
281 derived sequencing reads than the other two samples within the DeL9_12 group **(Fig. 1A)**.
282 Thus, we conclude that BIR1 levels contribute to creating heterogeneous transcriptomes
283 between replicates, although other factors such as the severity of the phenotypes caused by
284 BIR1 overexpression may also yield quantitative differences in their expression profiles.

285 Differentially expressed genes (DEG) from different comparisons are presented in **Table S3**. A
286 dramatic impact on the transcriptome was registered in plants that overexpress BIR1 (12 days
287 of DEX treatment) (adjusted *p*-value ≤ 0.05) **(Figs. S1B, S1C)**. Using stricter statistical
288 thresholds ($|\log_2(\text{Fold-Change})| \geq 1$ and adjusted *p*-value ≤ 0.01), 270 and 2,051 DEGs were
289 detected in BIR1 L9 plants after 4 and 12 days of DEX treatment, respectively, relative to the
290 mock-treated controls (DeL9_ vs MoL9_). Of them, 191 and 1,809 genes were up-regulated
291 and 79 and 242 were down-regulated **(Fig. 1C)** (**Table S4)**. 584 and 4,125 genes were distinctly
292 expressed between BIR1 L9 and WT plants after 4 and 12 days of DEX-treatment (DeL9_ vs
293 DeWT_), respectively, of which 220 and 1,815 genes were up-regulated and 364 and 2,310
294 were down-regulated **(Fig. 1C)** (**Table S4)**. These findings indicate that a massive
295 transcriptional reprogramming occurs when BIR1 is overexpressed in Arabidopsis but not when
296 BIR1 is transcriptionally induced at physiological levels.

297 Gene functional enrichment analysis was used to infer biological functions or pathways
298 significantly associated with DEGs. Gene ontology (GO) analysis showed that genes encoding
299 proteins with oxidoreductase activity, transmembrane transport and other metabolic processes
300 or genes related to lipid or carbohydrate metabolism were particularly overrepresented in our
301 whole set of DEGs, including WT and BIR1 L9 plants, after long DEX treatments **(Figs. 1D,**
302 **S1D, S2D) (Table S5)**. Notably, DEGs with kinase activity were only enriched in BIR1
303 overexpressing L9 plants, relative to mock-treated BIR1 L9 plants **(Figs. 1D, S1D)**. The kinase
304 activity GO term was not enriched in DEX- or mock-treated WT plants at any point tested,
305 excluding a DEX effect **(Fig. S2D)**. The Kyoto Encyclopedia of Genes and Genomes (KEGG)

306 pathway analysis showed the enrichment of genes related to several metabolic processes and
307 biosynthesis of secondary metabolites that were specifically regulated after DEX-treatments
308 **(Fig. S3) (Table S6)**. Conversely, DEGs involved in plant hormone signal transduction were
309 significantly enriched only in BIR1 overexpressing BIR1 L9, but not in mock-treated BIR1 L9
310 plants or WT plants exposed to DEX.

311 As indicated above, the implemented experimental approach further allowed us to study the
312 impact of DEX application. Macroscopically, WT plant treated with DEX for 12 days exhibited
313 identical morphology as the mock-treated controls but produced significantly smaller rosettes
314 due to the effects of DEX treatments **(Fig. S2A)**. Changes in gene expression due to DEX
315 treatments in WT plants are listed in **Table S4 (Fig. S2B)**. PCA analysis revealed that the
316 duration of the DEX treatment was the dominant source of variance underlying PC1 (36.80%)
317 in the PCA score plot **(Fig. S2C)**. GO and KEGG analyses revealed a significant enrichment of
318 terms related to oxidoreductase activities and metabolic processes in response to DEX
319 treatments **(Figs. S2D, S3)**.

320

321 **Effects of BIR1 induction on ROS and ethylene production and PTI gene expression in**
322 **response to bacterial elicitors**

323 We wanted to assess the effects of the physiological induction of BIR1 on early events of the
324 PTI response. BIR1 was induced by treating BIR1 plants with a 30 µM DEX solution 4 times
325 at 24h intervals, whereas control plants were mock-treated with H_2O. The luminol-based assay
326 showed that ROS production triggered by 1 µM flg22 was comparable between WT and BIR1
327 L6 and L9 plants **(Fig. 2A)**. Then, we tested the production of the phytohormone ethylene in
328 response to flg22 and nlp20 at concentrations of 1 µM and 100 nM. As expected, ethylene levels
329 were significantly increased in WT, BIR1 L6 and L9 plants in response to flg22 and, to a greater
330 extent, nlp20 at both concentrations tested. However, the induction of BIR1 in DEX-treated
331 plants had no measurable consequences on ethylene accumulation compared to the mock-
332 treated controls **(Fig. 2B)**. Next, we tested the expression of the canonical PTI marker genes
333 encoding FLG22-INDUCED RECEPTOR-LIKE KINASE 1 (FRK1) and PATHOGENESIS-
334 RELATED 1 (PR1) in BIR1 L6 and L9 transgenic plants upon 1 µM flg22 elicitation. Whereas
335 all these genes were significantly up-regulated in mock-treated controls (DEX-), BIR1
336 induction by DEX in BIR1 L6 an L9 plants notably reduced transcript levels (DEX+).
337 Importantly, PTI genes clearly responded to flg22 in WT plants regardless of DEX, which

338 discards a potential repressive effect of DEX on PTI gene expression **(Fig. 2C)**. The induction
339 of BIR1 protein in the BIR1 L6 and L9 plants used for ROS and ethylene assays was confirmed
340 by immunocapture followed by western blot, while BIR1 transcript levels were monitored in
341 the samples used for RT-qPCR expression assays (**Fig. 2D**).

342 Collectively, these results indicate that BIR1 induction within a physiological threshold
343 has negligible effects on ROS production or ethylene accumulation but interferes with
344 downstream events in the PTI pathway leading to transcriptional activation of defense genes.

345

346 **Induction of BIR1 hinders callose deposition at PD triggered by flg22 or dsRNA**

347 Callose-containing depositions at the cell-wall and PD triggered by conserved PAMPs occur
348 during the early stages of pathogen invasion (Luna *et al.*, 2011). Deposition of callose at PD
349 regulates symplastic transport, and limits the ability of the invading pathogen to enter plant
350 tissues (De Storme & Geelen, 2014; Xu *et al.*, 2017; Huang *et al.*, 2023). To investigate whether
351 physiological induction of BIR1 could affect PD callose deposition, we used *in vivo* aniline
352 blue staining to quantify PD-associated callose from digital photographs of BIR1 L9
353 Arabidopsis plants. BIR1 was induced with a 30 µM DEX solution 3 times at 24h intervals,
354 whereas control plants were mock-treated with H_2O. We first investigated callose deposition
355 using 1 µM flg22 as elicitor. Flg22 treatment of control (DEX-) BIR1 L9 plants caused a
356 noticeable increase in PD callose intensity compared to plants treated without elicitor (H_2O)
357 **(Figs. 3A, C)**. In contrast, PD-associated callose induced by flg22 remained at H_2O-induced
358 control levels in BIR1-expressing plants (DEX+) **(Figs. 3A, C)**, indicating that BIR1 was able
359 to interfere, at least partially, with PD callose deposition triggered by flg22.

360 To study if BIR1-mediated callose inhibition was a general response, BIR1 L9 plants were
361 treated with the synthetic dsRNA analog polyinosinic-polycytidylic acid [poly(I:C)] (0.5 µg μl^{-}
362 ^{1}) since dsRNA is known to trigger deposition of callose and PD closure in Arabidopsis (Huang
363 *et al.*, 2023). In the absence of DEX, callose intensity was significantly higher in BIR1 L9
364 plants treated with poly(I:C) compared to H_2O-treated plants. In contrast, after DEX treatment,
365 poly(I:C)-induced callose was significantly repressed by the expression of BIR1 (**Figs. 3B, C**).
366 Callose was enhanced in DEX-treated WT plants in response to poly(I:C) relative to H_2O-
367 treated plants, suggesting that DEX does not affect callose deposition in the WT genotype **(Fig.**
368 **3C)**. These findings indicate that the activation of BIR1 impairs PD callose deposition induced
369 by different PAMP elicitors.

370 We further explored if callose accumulation elicited by poly(I:C) or flg22 at the PD was
371 SOBIR1-dependent using a *sobir1-12* mutant (Gao *et al.*, 2009; Liu *et al.*, 2016). We observed
372 enhanced callose deposition in WT plants in response to poly(I:C), whereas the median PD
373 callose level detected in *sobir1-12* plants after poly(I:C) treatment was similar to those triggered
374 in H_2O-treated *sobir1-12* plants **(Fig. 3D)**. Surprisingly, PD callose deposition in the *sobir1-12*
375 background was also reduced in response to flg22 (**Fig. 3D**). Callose activation at PD by both
376 elicitors was inhibited in the double *bir1-1 sobir1-1* mutant **(Fig. 3D).** These findings indicate
377 that callose deposition triggered by either dsRNA or bacterial flg22 involved the SOBIR1 co-
378 receptor.

379

380 **BIR1 overexpression triggers the expression of immunity-related genes**

381 To independently validate the RNA-Seq results, we used RT-qPCR to examine the expression
382 of a subset of DEGs using independent sets (not used for RNA-seq) of mock- and DEX-treated
383 BIR1 L9 plants collected after 12 days of treatment. Our results indicated that expression of
384 BIR1, PR1, RESPIRATORY BURST OXIDASE HOMOLOG PROTEIN D (RBOHD), FRK1
385 and CYTOCHROME P450 MONOOXYGENASE 79B2 (CYP79B2) defense genes were all
386 significantly up-regulated in Arabidopsis plants overexpressing BIR1 compared to mock-
387 treated controls, which is in good consistency with their RNA-Seq-based expression profiles
388 **(Fig. 4A)**.

389 A detailed inspection of the RNA-Seq data revealed that multiple genes involved in the
390 perception of pathogens and the activation of downstream defense pathways were misregulated
391 when BIR1 was overexpressed. To increase accuracy, in the following analyses we have
392 considered solely DEGs with a $|\log_2 (\text{Fold-Change})| \geq 1$ and adjusted p-value ≤ 0.01. Genes
393 encoding LRR-type RLKs in the Arabidopsis genome were significantly enriched in response
394 to high levels of BIR1 [n= 225, two-tailed Fisher's exact test, P = 0.001 (DeL9_12 vs
395 DeWT_12) and P=4.5E-4 (DeL9_12 vs MoL9_12)] **(Table S7)**. Besides, cysteine-rich RLKs
396 (CRK), which contain cysteine-rich repeats in their extracellular domain, were highly
397 overrepresented in the pool of DEGs [n= 42, two-tailed Fisher's exact test, P = 1.06E-6
398 (DeL9_12 vs DeWT_12) and P=1.86E-9 (DeL9_12 vs MoL9_12)] **(Table S7) (Fig. S4)** (Chen,
399 2001). CRKs are important in the perception of apoplastic ROS and, likely in association with
400 BAK1, in the activation of PTI, enhanced pathogen resistance and hypersensitive response-
401 associated cell death (Yeh *et al.*, 2015; Quezada *et al.*, 2019; Castro *et al.*, 2021). Furthermore,

402 we observed a high percentage of RLP coding genes in Arabidopsis, not expected by chance,
403 in the list of DEGs [n=57, two-tailed Fisher's exact test, P = 4.08E-5 (DeL9_12 vs DeWT_12)
404 and P=6.04E-9 (DeL9_12 vs MoL9_12)] **(Table S7) (Fig. S5)** (Wang *et al.*, 2008; Lv *et al.*,
405 2016). Most of LRR-RLK, CRK and RLP transcripts were up-regulated in response to elevated
406 BIR1, but not in DEX-treated WT plants. RNA-Seq data revealed that BIR1 overexpression
407 boosted the transcription of many other genes involved in PTI and ETI signaling **(Figs. 4B,**
408 **S6A)**. This includes the RLK co-receptors BAK1 and SOBIR1, RLCKs such as BIK1 and
409 several AvrPphB SUSCEPTIBLE1(PBS1)-LIKE (PBL) (PBL4, PBL12, PBL20) (Liang &
410 Zhou, 2018; Rao *et al.*, 2018) **(Table S7)**. Active BIK1 positively regulates a Ca^{2+} influx from
411 apoplast to cytosol that induces a conformational change in CPKs that switches on their kinase
412 activity (Li *et al.*, 2014; Yip Delormel & Boudsocq, 2019). Collectively, CPKs were not
413 differentially regulated in plants overexpressing BIR1, but many individual CPKs were
414 regarded as DEGs in our assay. For instance, the expression of CPK4-6 and CPK11, which are
415 key players for transcriptional reprogramming upon elicitor perception, was enhanced only in
416 DEX-treated BIR1 L9 plants **(Fig. S6B)** (Boudsocq *et al.*, 2010). Upon ligand perception, BIK1
417 dissociates from activated receptor complexes and phosphorylates the plasma membrane
418 NADPH oxidase RBOHD to generate extracellular ROS (Kadota *et al.*, 2014; Li *et al.*, 2014;
419 Marcec & Tanaka, 2021). Interestingly, RBOHD was induced in DEX-treated BIR1 L9 plants
420 after both 4 and 12 days of treatment, but not in their corresponding controls **(Figs. 4A, 4B)**.
421 We found that elevated BIR1 levels strongly increased the transcript abundance of genes
422 encoding the lipase-like proteins EDS1, PHYTOALEXIN DEFICIENT 4 (PAD4),
423 SENESCENCE ASSOCIATED-GENE 101 (SAG101) and ACTIVATED DISEASE
424 RESISTANCE 1 (ADR1), which are required for TNL-receptor function during ETI **(Figs.**
425 **4B)** (Zhou & Zhang, 2020; Ngou *et al.*, 2021; Pruitt *et al.*, 2021b; Sun *et al.*, 2021; Tian *et al.*,
426 2021). Accordingly, a large number of DEGs in our assay were annotated as disease resistance
427 (R) protein-coding genes, of which the TNL class was particularly enriched [n=100, two-tailed
428 Fisher's exact test, P = 0.06 (DeL9_12 vs DeWT_12) and P=4.4E-5 (DeL9_12 vs MoL9_12)]
429 (Swiderski *et al.*, 2009) **(Table S7)**. Conversely, neither NON-RACE SPECIFIC DISEASE
430 RESISTANCE 1 (NDR1) nor genes encoding CNL intracellular receptors, which require
431 NDR1, were differentially expressed in response to BIR1 overexpression **(Fig. 4B) (Table S3)**.
432 EDS5, which transduces downstream of SA in Arabidopsis (Nawrath *et al.*, 2002), was highly
433 up-regulated in a BIR1-dependent manner. Interestingly, BIR2 was distinctively up-regulated
434 in DEX-treated BIR1 L9 samples, whereas BIR3 and its partner CONSTITUTIVE SHADE
435 AVOIDANCE 1 (CSA1), which also interacts with BIR1, were unaffected in plants

436 overexpressing BIR1 **(Fig. S6A)** (Schulze *et al.*, 2022). Consistent with transcript levels,
437 SOBIR1, PAD4-dependent PR1 and EDS1 proteins were strongly up-regulated by BIR1
438 overexpression in DEX-treated BIR1 L9 plants, compared to the non-treated controls (**Figs.**
439 **4C, 5C**).

440 In conclusion, our data indicated that the overexpression of BIR1 significantly alters hormone
441 homeostasis and up-regulates multiple immune receptors and co-receptors involved in the
442 perception and signaling of ligands and effectors. Defense activation in BIR1 overexpressing
443 plants occurs in the absence of microbes or microbe-derived elicitors/effectors, and correlates
444 with growth phenotypes and cell death that are reminiscent of plants with constitutively
445 activated defenses (Lorrain *et al.*, 2003; Guzman-Benito *et al.*, 2019).

446

447 **Genetic disruption of SOBIR1, but not BAK1, partially rescues BIR1 overexpression**
448 **phenotypes**

449 SOBIR1 and BAK1 are necessary for activating cell death and constitutive defense responses
450 in the knock-out *bir1-1* mutant (Gao *et al.*, 2009; Liu *et al.*, 2016). Therefore, we tested if
451 SOBIR1 and BAK1 were also required for the phenotypes associated with non-physiological
452 doses of BIR1. A DEX-inducible BIR1-mCherry system was used to generate independent
453 homozygous transgenic lines in the well-characterized *sobir1-12* and *bak1-5* mutant
454 backgrounds (Gao *et al.*, 2009; Schwessinger *et al.*, 2011). Transgenic plants were sprayed with
455 30 µM DEX solution or H_2O (mock-treated controls) for 12 days at 24 h intervals to promote
456 BIR1 overexpression.

457 As previously shown, our reference set of DEX-treated BIR1 L9 plants accumulated high levels
458 of BIR1 transcripts, and displayed a range of stunting symptoms, accelerated senescence
459 (yellowing), and cell death relative to non-treated BIR1 L9 controls or DEX-treated WT plants
460 **(Fig. 5A)** (Guzman-Benito *et al.*, 2019). Nonetheless, growth retardation in DEX-treated plants
461 was partially due to DEX effects as shown for WT plants after 12 days of DEX treatment **(Fig.**
462 **5A)**. When *sobir1-12* BIR1 plants were investigated, we observed that the phenotypes after 12
463 days of DEX treatments, albeit variable between biological replicates, were milder than those
464 in BIR1 L9 plants, and ranged from typical WT appearance to localized yellowing and,
465 occasionally, discrete leaf necrosis **(Figs. 5A, S7A, S7B)**. Interestingly, BIR1 transcript and
466 protein accumulated in *sobir1-12* BIR1 plants like in BIR1 L9 plants after 12 days of DEX
467 application, discarding potential dose effects **(Fig. 5B, C)**. Furthermore, transcripts of the PTI-

468 markers RBOHD, FRK1 and WRKY DNA-BINDING PROTEIN 29 (WRK29) in DEX-treated
469 *sobir1-12* BIR1 plants, although slightly increased, were statistically indistinguishable from
470 non-treated controls **(Figs. 5D, S7C)**, suggesting that the up-regulation of PTI genes due to
471 BIR1 overexpression was affected by the lack of SOBIR1.

472 *bak1*-5 BIR1 plants consistently developed strong morphological phenotypes after 12 days of
473 DEX application, that closely resemble those of BIR1 L9 plants **(Figs. 5A, S7A, S7B)**. RT-
474 qPCR showed that BIR1 transcripts also accumulated in these plants after long DEX treatments,
475 although to a variable degree depending on the transgenic lines and biological replicates. For
476 instance, BIR1 transcript levels in *bak1*-5 BIR1 plants were comparable to those in *sobir1-12*
477 BIR1 plants in **Fig. S7B**. Besides, differences in BIR1 protein accumulation were observed
478 between DEX-treated *bak1-5* BIR1 L4 and L10 lines in this experiment **(Fig. 5C)**. Conversely,
479 **Figs. 5A** and **B** illustrate data from a different experimental replicate in which BIR1 transcripts
480 in *bak1*-5 BIR1 plants were much less abundant than in BIR1 L9 plants. These interesting
481 observations suggest that the persistent induction of BIR1 over time, rather than an excess of
482 BIR1, was the trigger of the morphological alterations in the *bak1*-5 mutant background.
483 RBOHD, FRK1 and WRKY remained transcriptionally up-regulated in DEX-treated *bak1-5*
484 BIR1 plants as they did in BIR1 L9 plants **(Figs. 5E)**. Collectively, these data indicate that the
485 morphological phenotypes and the activation of PTI defense genes that occur when BIR1 is
486 continually induced or overexpressed were partially dependent on SOBIR1, but genetically
487 unrelated to BAK1.

488 Alterations in plant hormone pathways may negatively affect plant growth (Denance *et al.*,
489 2013). The transcriptional reprogramming of genes involved in plant hormone metabolism and
490 signaling in BIR1-overexpressing plants prompted us to further examine their expression in the
491 mutant backgrounds mentioned above. RT-qPCR revealed that genes encoding salicylic acid
492 (SA)-dependent PR1, jasmonic acid (JA)-responsive PLANT DEFENSIN 1.2 (PDF1.2),
493 ethylene (ET)- and JA-responsive PR4 as well as genes encoding the cytochrome P450 enzymes
494 CYP71B15 (PAD3) and CYP79B2 involved in camalexin (CA)-biosynthesis and CA-mediated
495 plant defense, were all up-regulated in BIR1-overexpressing plants of *sobir1-12* BIR1
496 genotypes **(Fig. 5F)**. Intriguingly, the induction of these genes was notably reduced in *bak1-5*
497 BIR1 plants after DEX treatment compared to *sobir1-12* BIR1 or BIR1 L9 plants **(Fig. 4A,**
498 **5G)**. This data suggests that the *bak1-5* mutation may compromise, at least partially, defense
499 hormone signaling upon BIR1 overexpression. None of these genes, except PR1, were induced

500 or repressed in DEX-treated WT plants, discarding a potential effect of DEX on their expression
501 **(Table S3)**.

502

503 **Genetic disruption of EDS1, but not PAD4, partially rescues BIR1 overexpression**
504 **phenotypes**

505 A previous report showed that growth stunting, activation of cell death and defense responses
506 in the *bir1-1* mutant are partially dependent on EDS1 and PAD4 (Gao *et al.*, 2009). The EDS1-
507 PAD4 node has a relevant role in PRR signaling and TNL activation, indicating that it mediates
508 both PTI and ETI (Pruitt *et al.*, 2021a). Given that TNL-coding transcripts were abundant in
509 BIR1 L9 plants and that EDS1 transcripts and protein were elevated in BIR1 L9, *sobir1-12*
510 BIR1 and *bak1-5* BIR1 plants (**Figs. 5B, C**), we wondered if TNL-mediated ETI responses
511 along with, or independently of, PTI could be important for BIR1 overexpression phenotypes.
512 Thus, we tested if the phenotypes caused by sustained BIR1 induction were dependent on EDS1
513 or PAD4. The DEX-inducible BIR1-mCherry system was used to generate homozygous
514 transgenic lines from *eds1-2* and *pad4-1* mutants (Parker *et al.*, 1996; Zhou *et al.*, 1998). The
515 *eds1-2* BIR1 plants displayed mostly WT-like morphologies and, occasionally, localized
516 yellowing after 12 days of DEX treatments compared to non-treated plants **(Figs. 6A, S7A)**.
517 Importantly, RT-qPCR analysis showed that BIR1 accumulated in the *eds1-2* BIR1 plants as
518 much as in the BIR1 L9 plants **(Figs. 6A)**. The expression of FRK1 and RBOHD was
519 significantly enhanced in *eds1-2* BIR1 plants after DEX applications compared to non-treated
520 controls **(Fig. 6B)**. Our data indicate that the lack of EDS1 attenuates the morphological
521 phenotypes caused by BIR1 overexpression, and pose the possibility that these phenotypic
522 alterations and the activation of PTI genes are unconnected processes.

523 Next, we found that *pad4-1* BIR1 plants had essentially BIR1 L9-like phenotypes after 12 days
524 of DEX applications **(Figs. 6A, S7A)**. In these plants, BIR1 accumulated much less than in
525 BIR1 L9 or *eds1-2* BIR1 plants **(Fig. 6A)**. As shown for *bak1-5* BIR1 plants, we presume that
526 sustained induction of BIR1, rather than BIR1 overexpression, was sufficient to cause typical
527 BIR1 phenotypes regardless of the *pad4-1* mutation. Interestingly, PTI-components FRK1,
528 WRKY29 and RBOHD showed no responsiveness to BIR1 overexpression in *pad4-1* BIR1
529 plants, which support the idea that cell death and PTI activation are unrelated in these plants
530 **(Figs. 6C, S7C)**. In summary, we observed that the genetic elimination of EDS1, but not PAD4,
531 contributes to mitigating the morphological phenotypes caused by continuous BIR1

532 induction/overexpression, and suggests that symptoms arise from the activation of EDS1-
533 dependent ETI-type cell death rather than the disruption of PRR-mediated PTI responses.

534 RT-qPCR revealed a significant transcriptional activation of marker genes in the SA, JA, ET
535 and CA pathways in response to high levels of BIR1 in DEX-treated *eds1-2* BIR1 plants versus
536 non-treated controls **(Fig. 6D)**. On the contrary, the same markers were poorly or no longer up-
537 regulated in *pad4*-1 BIR1 transgenics after 12 days of DEX treatments relative to the non-
538 treated controls, suggesting that PAD4 is important for PTI gene expression and phytohormone
539 homeostasis **(Fig. 6E)**.

540

541 **Phenotypes of BIR1 overexpressing lines are unrelated to SA signaling pathways**

542 Previously, high SA levels were found as partly responsible for *bir1-1* phenotypes (Gao *et al.*,
543 2009). However, *pad4-1* BIR1 plants were as sensitive as BIR1 L9 plants to DEX treatments,
544 suggesting that morphological phenotypes caused by non-physiological BIR1 levels are
545 independent of SA-mediated signaling. To confirm this prediction, the effects of mutations in
546 the SA biosynthesis on the growth and defense activation in BIR1 overexpressing plants were
547 assessed. In Arabidopsis, SALICYLIC ACID INDUCTION DEFICIENT
548 2/ISOCHORISMATE SYNTHASE 1 (SID2/ICS1) and EDS5 are involved in pathogen-
549 induced SA biosynthesis (Huang *et al.*, 2020). Therefore, DEX-inducible BIR1-mCherry
550 transgenics were generated in the *sid2-2* and *eds5-3* genetic backgrounds. We found that *sid2-*
551 *2* BIR1 plants exhibited from moderate to severe morphological phenotypes after 12 days of
552 DEX treatment that coincided with moderate levels of BIR1 overexpression relative to those
553 observed in BIR1 L9 plants **(Figs. 7A, B)**. *eds5*-3 BIR1 plants typically displayed strong
554 developmental defects and necrosis and accumulated BIR1 transcripts at BIR1 L9 levels after
555 long DEX applications **(Figs. 7A, C)**. The transcription levels of PDF1.2 and CYP79B2, but
556 not PAD3, were high in DEX-treated *sid2*-2 BIR1 plants compared to non-treated controls **(Fig.**
557 **7B)**, while PAD3 and PDF1.2, but not CYP79B2 were up-regulated in *eds5-3* BIR1
558 overexpressing plants relative to non-treated controls **(Fig. 7C)**. Our findings confirm that the
559 phenotypical alterations linked to BIR1 overexpression were not drastically affected by
560 disruptive mutations in SA biosynthesis (*sid2-2* and *eds5-3*) and SA signaling (*pad4-1*).

561

562 **Discussion**

563 Plants respond to microbes and viruses by enhancing the expression of multiple genes that
564 function as regulators or executors of various defense programs (Nishad *et al.*, 2020). Among
565 them, BIR1 was shown to be up-regulated during bacterial and oomycete infections, and during
566 viral infections in a SA-dependent manner (Gao *et al.*, 2009; Guzman-Benito *et al.*, 2019). The
567 observation that knock-out *bir1-1* mutants have increased resistance to the virulent oomycete
568 *Hyaloperonospora parasitica* Noco2 and to the RNA virus *Tobacco rattle virus* (TRV) suggests
569 an active role in plant immunity (Gao *et al.*, 2009; Guzman-Benito *et al.*, 2019). Since BIR1 is
570 a negative regulator of cell death and defense (Liu *et al.*, 2016; Ma *et al.*, 2017), we
571 hypothesized that BIR1 induction might be part of a common strategy to modulate, at least
572 partially, the amplitude of the immune responses during microbial and viral infections. To test
573 the hypothesis, we used a previously described DEX-inducible system for the conditional
574 expression of a mCherry-tagged BIR1 transgene in Arabidopsis (Guzman-Benito *et al.*, 2019).
575 This system allowed us to investigate the outputs associated with short and long BIR1 induction
576 times. Importantly, BIR1 induction is triggered in the absence of immune elicitors or effectors
577 that could otherwise initiate undesirable localized and systemic defense responses in the plant.
578 Upon short-term DEX treatments, BIR1 accumulates in rosette leaves to levels comparable to
579 those observed under natural conditions in bacteria- or virus-infected plants, or plants treated
580 with SA (Gao *et al.*, 2009; Guzman-Benito *et al.*, 2019). In the absence of pathogens or elicitors,
581 short induction of BIR1 has a subtle, if any, impact on both plant transcriptome and plant
582 morphology. In contrast, in the presence of the PTI elicitor flg22, the physiological induction
583 of BIR1 negatively affects the expression of several PTI-marker genes, whereas it has no effects
584 on ROS burst, as previously shown (Liu *et al.*, 2016), or production of ethylene. This
585 observation suggests that BIR1 can regulate, directly or indirectly, the activity of components
586 in the PTI signaling pathway that ultimately control immune gene transcription. Likewise, BIR1
587 activation compromises the callose deposition at PD elicited by either flg22 or the dsRNA-
588 analog poly(I:C). PD allow cell-to-cell and long-distance transport of micro- and
589 macromolecules, representing gateways through which plant viruses pass from cell to cell to
590 spread infections (De Storme & Geelen, 2014). Targeted deposition of callose modulates
591 symplastic connectivity by regulating PD pore size, and therefore constitutes an essential layer
592 in the defense against pathogens (Wang *et al.*, 2021). According to our data, induction of BIR1
593 during pathogen attack can be interpreted as a strategy to regulate PD trafficking. Although not
594 tested in this study, BIR1 effects on gene expression and callose deposition may render PTI less
595 effective against pathogens. Indeed, PTI gene expression and callose formation are usually
596 blocked/inhibited by many defense-suppressing virulence effectors from different types of

597 microbes (Cui *et al.*, 2009; Wang *et al.*, 2021). Viral-encoded proteins such as the potyviral
598 silencing suppressor helper-component proteinase (HC-Pro) or the movement protein (MP) of
599 several tobamoviruses are capable of suppressing callose deposition (Citovsky *et al.*, 1990;
600 Chowdhury *et al.*, 2020). A recent work shows that tobamovirus MPs promote viral cell-to-cell
601 propagation by blocking dsRNA-induced callose deposition (Huang *et al.*, 2023). It is tempting
602 to speculate that BIR1 induction during the viral infection controls PD callose deposition, and
603 perhaps other antiviral defenses, triggered by viral-derived dsRNA. dsRNA-induced deposition
604 of callose requires PTI signaling components such as SERK1 and BIK1/PBL1 (Huang *et al.*,
605 2023). Our results show that PD callose deposition elicited by flg22 or poly(I:C) is inhibited in
606 the *sobir1-1* mutant. This observation is puzzling because flg22 signaling is independent of
607 SOBIR1. Further research is needed to understand the role of SOBIR1 in controlling PD callose
608 deposition.

609 Long DEX treatments of BIR1 transgenic plants led to sustained and/or elevated BIR1 levels
610 (non-physiological) similar to those expected if BIR1 gene regulation were lost. Under these
611 conditions, plants exhibit dramatic changes in gene expression and eventually strong
612 morphological and growth phenotypes, including accelerated senescence (yellowing), stunting,
613 necrosis and cell death (Guzman-Benito *et al.*, 2019). An excess of BIR1 in our transgenic
614 plants also induced the activation of multiple genes involved in different branches of the PTI
615 and ETI signaling responses. Among them, the up-regulation of a significant number of RLP-
616 coding genes is striking. RLPs have been observed predominantly expressed in senescence
617 leaves, supporting the idea that BIR1 overexpression accelerates a senescence program (Wang
618 *et al.*, 2008). In Arabidopsis, RLP1, RLP23, RLP30, RLP32 and RLP42 mediate SOBIR1-
619 dependent immune activation, but the role of other RLPs in the perception of pathogen and
620 defense is unknown (Wang *et al.*, 2008; Zhang *et al.*, 2013; Albert *et al.*, 2019). The
621 overexpression of genes encoding TNL-resistance proteins, but not CNLs, is another important
622 feature linked to high levels of BIR1. Here, we provide genetic evidence that morphological
623 phenotypes due to persistent BIR1 induction are partially dependent on EDS1. TNL-based
624 immunity is mediated by two distinct signaling modules, EDS1/SAG101/NRG1 and
625 EDS1/PAD4/ADR1 (Sun *et al.*, 2021). Since knocking out PAD4 had little influence on BIR1
626 overexpression phenotypes, we propose that EDS1, perhaps in concert with SAG101, triggers
627 cell death-like phenotypes upon TNL activation in BIR1 overexpressing plants **(Fig. 7D)**. How
628 TNL receptors are activated when BIR1 is strongly expressed is a question to resolve. A current
629 model postulates that loss of BIR1 function leads to the activation of hypothetical guarding R

630 proteins which further feed PAD4- and SOBIR1-dependent resistance pathways (Gao *et al.*,
631 2009). Our results are also coherent with BIR1 or a yet unknown BIR1/SERK complex being
632 guarded by one or several EDS1-dependent TNL proteins. Therefore, non-physiological
633 induction of BIR1 may promote TNL-mediated resistance pathways that require EDS1 when
634 no effectors or elicitors are present. In addition to EDS1, we demonstrated that SOBIR1 is
635 necessary for BIR1 overexpression phenotypes. The role of SOBIR1 in the BIR1 pathway is
636 unclear. Although extensive investigation is required, SOBIR1 may function as a specific co-
637 regulator of the EDS1-dependent responses triggered by BIR1 overexpression, as part of the
638 same signaling pathway **(Fig. 7D)**. This idea is inspired by a recent work showing that the cell-
639 surface RLP23 receptor uses SOBIR1 to form a supramolecular complex with a
640 EDS1/PAD4/ADR1 node in a ligand-independent manner to mediate defense signaling
641 cascades that are common to both surface PRR (PTI) and NLR (ETI) receptors (Pruitt *et al.*,
642 2021b). The TNL protein CSA1 senses perturbances of BIR3, BAK1 or BIR3/BAK1
643 complexes leading to ETI-type autoimmune responses (Schulze *et al.*, 2022). CSA1 did not
644 show responsiveness to BIR1 overexpression in our assay, but it has been shown to interact
645 with BIR1 (Schulze *et al.*, 2022). It will be interesting to see if CSA1 also guards BIR1 integrity,
646 perhaps in cooperation with SOBIR1 and/or other SERKs **(Fig. 7D)**. Finally, phenotypes linked
647 to BIR1 overexpression were apparently unaffected by the *bak1-5* mutation, which suggests
648 that other SERK family members can compensate for the loss of BAK1 in PTI/ETI signaling.

649 We observed that the up-regulation of FRK1, WRKY29 and RBOHD due to BIR1
650 overexpression was compromised by mutations in SOBIR1 and PAD4, but it was independent
651 of EDS1. Since EDS1, PAD4 and SOBIR1 are important for both cell surface PRR receptor-
652 and TNL-mediated signaling and resistance (Pruitt *et al.*, 2021b; Tian *et al.*, 2021), we will
653 need additional experimentation to establish if changes in PTI gene expression involve PTI-
654 dependent pathways, TNL activation or other unknown mechanisms yet to be determined. Our
655 study also revealed significant alterations in plant hormone gene expression. Interestingly,
656 genes related to the plant hormones ET, JA, CA, and SA, which play a central role in regulating
657 immune responses, remained up-regulated in *eds1-2* BIR1 and *sobir1-12* BIR1 backgrounds,
658 in which phenotypes were partially rescued. This suggests that i) regulation of hormone
659 homeostasis does not require SOBIR1- and/or EDS1-mediated signaling pathways, and that ii)
660 such hormonal imbalance has little, if any, influence on the ETI-like phenotypes observed in
661 BIR1 overexpressing plants.

662

663 **Conclusions**

664 Here, we investigated the implications of BIR1 homeostasis on the immune response in
665 Arabidopsis. BIR1 induction at physiological levels interferes with both immune gene
666 expression and PD callose deposition triggered by canonical PTI elicitors. We posit that BIR1
667 induction may represent a pathogen-driven mechanism to modulate plant defenses, and that this
668 mechanism helps to maintain a host-pathogen equilibrium during infections. Over time
669 induction of BIR1 typically leads to high levels on BIR1 in the plant tissue, and causes severe
670 morphological and growth defects concomitant with transcriptomic changes affecting plant
671 immunity. These findings indicate a dose-dependency of the BIR1 regulatory activity, in which
672 persistent BIR1 induction/BIR1 overexpression over time results in autoimmunity and fitness
673 penalties. We provide experimental evidence that both EDS1 and SOBIR1, but neither PAD4
674 nor BAK1, were necessary for the ETI-type cell death phenotypes that occur when BIR1 is
675 overexpressed. We hypothesize that one or several unknown TNLs monitor the integrity of
676 BIR1 or BIR1-co-receptor complexes and that SOBIR1 cooperates with EDS1 to transduce
677 signals downstream of TNL **(Fig. 7D)**.

678

679 **Acknowledgements**

680 This work was supported by National Research grants RTI2018-096979-B-I00 and PID2021
681 7982NB-I00 to CL from Ministerio de Ciencia e Innovación (Spain) and UE-FEDER, and grant
682 iLINKA20415 to CL from CSIC (Spain). Contributions of ARS, LEG and MH were supported
683 by grants ERA-NET SusCrop2 / ANR-21-SUSC-0003-01 and ANR-PRC / ANR-21-CE20-
684 0020-01 to MH. Contributions of CH and TN were supported by DFG grant Nu70/17-1 to TN.
685 We thank Rosa Lozano-Durán, Birgit Kemmerling, Laura Medina-Puche and Delphine Pott for
686 critical reading and colleagues who kindly donated seeds and materials.

687

688 **Author contributions**

689 CL and IGB conceived and designed the study. CL, IGB, CR and IP performed expression
690 assays and transgenics. CL and CH performed ROS and ethylene assays. CL, ARS and LEG
691 performed callose assays. CL, IGB, MH and TN analyzed the data. CL wrote the article.

692

693 **REFERENCES**

694 **Albert I, Bohm H, Albert M, Feiler CE, Imkampe J, Wallmeroth N, Brancato C,**
695 **Raaymakers TM, Oome S, Zhang H, et al. 2015.** An RLP23-SOBIR1-BAK1 complex
696 mediates NLP-triggered immunity. *Nat Plants* **1**: 15140.
697 **Albert I, Zhang L, Bemm H, Nurnberger T. 2019.** Structure-function analysis of immune
698 receptor AtRLP23 with its ligand nlp20 and coreceptors AtSOBIR1 and AtBAK1. *Mol*
699 *Plant Microbe Interact* **32**(8): 1038-1046.
700 **Belkhadir Y, Jaillais Y, Epple P, Balsemao-Pires E, Dangl JL, Chory J. 2012.**
701 Brassinosteroids modulate the efficiency of plant immune responses to microbe-associated
702 molecular patterns. *Proc Natl Acad Sci U S A* **109**(1): 297-302.
703 **Bi G, Zhou Z, Wang W, Li L, Rao S, Wu Y, Zhang X, Menke FLH, Chen S, Zhou JM.**
704 **2018.** Receptor-like cytoplasmic kinases directly link diverse pattern recognition Receptors
705 to the activation of mitogen-activated protein kinase cascades in Arabidopsis. *Plant Cell*
706 **30**(7): 1543-1561.
707 **Boudsocq M, Willmann MR, McCormack M, Lee H, Shan L, He P, Bush J, Cheng SH,**
708 **Sheen J. 2010.** Differential innate immune signalling via Ca(2+) sensor protein kinases.
709 *Nature* **464**(7287): 418-422.
710 **Boutrot F, Zipfel C. 2017.** Function, discovery, and exploitation of plant pattern recognition
711 receptors for broad-spectrum disease resistance. *Annu Rev Phytopathol* **55**: 257-286.
712 **Castro B, Citterico M, Kimura S, Stevens DM, Wrzaczek M, Coaker G. 2021.** Stress-
713 induced reactive oxygen species compartmentalization, perception and signalling. *Nat*
714 *Plants* **7**(4): 403-412.
715 **Chen Z. 2001.** A superfamily of proteins with novel cysteine-rich repeats. *Plant Physiol* **126**(2):
716 473-476.
717 **Chowdhury RN, Lasky D, Karki H, Zhang Z, Goyer A, Halterman D, Rakotondrafara**
718 **AM. 2020.** HCPro suppression of callose deposition contributes to strain-specific
719 resistance against Potato Virus Y. *Phytopathology* **110**(1): 164-173.
720 **Citovsky V, Knorr D, Schuster G, Zambryski P. 1990.** The P30 movement protein of tobacco
721 mosaic virus is a single-strand nucleic acid binding protein. *Cell* **60**(4): 637-647.
722 **Clough SJ, Bent AF. 1998.** Floral dip: a simplified method for Agrobacterium-mediated
723 transformation of Arabidopsis thaliana. *Plant J* **16**(6): 735-743.
724 **Couto D, Zipfel C. 2016.** Regulation of pattern recognition receptor signalling in plants. *Nat*
725 *Rev Immunol* **16**(9): 537-552.
726 **Cui H, Xiang T, Zhou JM. 2009.** Plant immunity: a lesson from pathogenic bacterial effector
727 proteins. *Cell Microbiol* **11**(10): 1453-1461.

728 **De Storme N, Geelen D. 2014.** Callose homeostasis at plasmodesmata: molecular regulators
729 and developmental relevance. *Front Plant Sci* **5**: 138.
730 **Denance N, Sanchez-Vallet A, Goffner D, Molina A. 2013.** Disease resistance or growth: the
731 role of plant hormones in balancing immune responses and fitness costs. *Front Plant Sci*
732 **4**: 155.
733 **Dominguez-Ferreras A, Kiss-Papp M, Jehle AK, Felix G, Chinchilla D. 2015.** An overdose
734 of the Arabidopsis coreceptor BRASSINOSTEROID INSENSITIVE1-ASSOCIATED
735 RECEPTOR KINASE1 or its ectodomain causes autoimmunity in a SUPPRESSOR OF
736 BIR1-1-dependent manner. *Plant Physiol* **168**(3): 1106-1121.
737 **Fernandez-Calvino L, Guzman-Benito I, Del Toro FJ, Donaire L, Castro-Sanz AB, Ruiz-**
738 **Ferrer V, Llave C. 2016.** Activation of senescence-associated Dark-inducible (DIN) genes
739 during infection contributes to enhanced susceptibility to plant viruses. *Mol Plant Pathol*
740 **17**(1): 3-15.
741 **Gao M, Wang X, Wang D, Xu F, Ding X, Zhang Z, Bi D, Cheng YT, Chen S, Li X, et al.**
742 **2009.** Regulation of cell death and innate immunity by two receptor-like kinases in
743 Arabidopsis. *Cell Host Microbe* **6**(1): 34-44.
744 **Gust AA, Pruitt R, Nurnberger T. 2017.** Sensing danger: key to activating plant immunity.
745 *Trends Plant Sci* **22**(9): 779-791.
746 **Guzman-Benito I, Donaire L, Amorim-Silva V, Vallarino JG, Esteban A, Wierzbicki AT,**
747 **Ruiz-Ferrer V, Llave C. 2019.** The immune repressor BIR1 contributes to antiviral
748 defense and undergoes transcriptional and post-transcriptional regulation during viral
749 infections. *New Phytol* **224**(1): 421-438.
750 **Halter T, Imkampe J, Mazzotta S, Wierzba M, Postel S, Bucherl C, Kiefer C, Stahl M,**
751 **Chinchilla D, Wang X, et al. 2014.** The leucine-rich repeat receptor kinase BIR2 is a
752 negative regulator of BAK1 in plant immunity. *Curr Biol* **24**(2): 134-143.
753 **Hohmann U, Lau K, Hothorn M. 2017.** The structural basis of ligand perception and signal
754 activation by receptor kinases. *Annu Rev Plant Biol* **68**: 109-137.
755 **Huang C, Mutterer J, Heinlein M. 2022.** In vivo aniline blue staining and semiautomated
756 quantification of callose deposition at plasmodesmata. *Methods Mol Biol* **2457**: 151-165.
757 **Huang C, Sede AR, Elvira-González L, Yan Y, Rodriguez M, Mutterer J, Boutant E, Shan**
758 **L, Heinlein M. 2023.** dsRNA-induced immunity targets plasmodesmata and is suppressed
759 by viral movement proteins. *Plant Cell* https://doi.org/10.1101/2022.11.21.517408.
760 **Huang W, Wang Y, Li X, Zhang Y. 2020.** Biosynthesis and regulation of salicylic acid and
761 N-hydroxypipecolic acid in plant immunity. *Mol Plant* **13**(1): 31-41.

762 **Imkampe J, Halter T, Huang S, Schulze S, Mazzotta S, Schmidt N, Manstretta R, Postel**
763 **S, Wierzba M, Yang Y, et al. 2017.** The Arabidopsis leucine-rich repeat receptor kinase
764 BIR3 negatively regulates BAK1 receptor complex formation and stabilizes BAK1. *Plant*
765 *Cell* **29**(9): 2285-2303.
766 **Jubic LM, Saile S, Furzer OJ, El Kasmi F, Dangl JL. 2019.** Help wanted: helper NLRs and
767 plant immune responses. *Curr Opin Plant Biol* **50**: 82-94.
768 **Kadota Y, Sklenar J, Derbyshire P, Stransfeld L, Asai S, Ntoukakis V, Jones JD, Shirasu**
769 **K, Menke F, Jones A, et al. 2014.** Direct regulation of the NADPH oxidase RBOHD by
770 the PRR-associated kinase BIK1 during plant immunity. *Mol Cell* **54**(1): 43-55.
771 **Korner CJ, Klauser D, Niehl A, Dominguez-Ferreras A, Chinchilla D, Boller T, Heinlein**
772 **M, Hann DR. 2013.** The immunity regulator BAK1 contributes to resistance against
773 diverse RNA viruses. *Mol Plant Microbe Interact* **26**(11): 1271-1280.
774 **Lee DH, Lee HS, Belkhadir Y. 2021.** Coding of plant immune signals by surface receptors.
775 *Curr Opin Plant Biol* **62**: 102044.
776 **Li L, Li M, Yu L, Zhou Z, Liang X, Liu Z, Cai G, Gao L, Zhang X, Wang Y, et al. 2014.**
777 The FLS2-associated kinase BIK1 directly phosphorylates the NADPH oxidase RbohD to
778 control plant immunity. *Cell Host Microbe* **15**(3): 329-338.
779 **Li P, Lu YJ, Chen H, Day B. 2020.** The Lifecycle of the plant immune system. *CRC Crit Rev*
780 *Plant Sci* **39**(1): 72-100.
781 **Liang X, Zhou JM. 2018.** Receptor-like cytoplasmic kinases: central players in plant receptor
782 kinase-mediated signaling. *Annu Rev Plant Biol* **69**: 267-299.
783 **Liebrand TW, van den Burg HA, Joosten MH. 2014.** Two for all: receptor-associated kinases
784 SOBIR1 and BAK1. *Trends Plant Sci* **19**(2): 123-132.
785 **Liu Y, Huang X, Li M, He P, Zhang Y. 2016.** Loss-of-function of Arabidopsis receptor-like
786 kinase BIR1 activates cell death and defense responses mediated by BAK1 and SOBIR1.
787 *New Phytol* **212**(3): 637-645.
788 **Lorrain S, Vailleau F, Balague C, Roby D. 2003.** Lesion mimic mutants: keys for deciphering
789 cell death and defense pathways in plants? *Trends Plant Sci* **8**(6): 263-271.
790 **Luna E, Pastor V, Robert J, Flors V, Mauch-Mani B, Ton J. 2011.** Callose deposition: a
791 multifaceted plant defense response. *Mol Plant Microbe Interact* **24**(2): 183-193.
792 **Lv Y, Yang N, Wu J, Liu Z, Pan L, Lv S, Wang G. 2016.** New insights into receptor-like
793 protein functions in Arabidopsis. *Plant Signal Behav* **11**(7): e1197469.

794 **Ma C, Liu Y, Bai B, Han Z, Tang J, Zhang H, Yaghmaiean H, Zhang Y, Chai J. 2017.**
795 Structural basis for BIR1-mediated negative regulation of plant immunity. *Cell Res* **27**(12):
796 1521-1524.
797 **Macho AP, Lozano-Duran R. 2019.** Molecular dialogues between viruses and receptor-like
798 kinases in plants. *Mol Plant Pathol* **20**(9): 1191-1195.
799 **Marcec MJ, Tanaka K. 2021.** Crosstalk between calcium and ROS signaling during flg22-
800 triggered immune response in Arabidopsis leaves. *Plants (Basel)* **11**(1).
801 **McHale L, Tan X, Koehl P, Michelmore RW. 2006.** Plant NBS-LRR proteins: adaptable
802 guards. *Genome Biol* **7**(4): 212.
803 **Mithoe SC, Menke FL. 2018.** Regulation of pattern recognition receptor signalling by
804 phosphorylation and ubiquitination. *Curr Opin Plant Biol* **45**(Pt A): 162-170.
805 **Nawrath C, Heck S, Parinthawong N, Metraux JP. 2002.** EDS5, an essential component of
806 salicylic acid-dependent signaling for disease resistance in Arabidopsis, is a member of the
807 MATE transporter family. *Plant Cell* **14**(1): 275-286.
808 **Ngou BPM, Ahn HK, Ding P, Jones JDG. 2021.** Mutual potentiation of plant immunity by
809 cell-surface and intracellular receptors. *Nature* **592**(7852): 110-115.
810 **Ngou BPM, Ding P, Jones JDG. 2022.** Thirty years of resistance: Zig-zag through the plant
811 immune system. *Plant Cell* **34**(5): 1447-1478.
812 **Nishad R, Ahmed T, Rahman VJ, Kareem A. 2020.** Modulation of plant defense system in
813 response to microbial interactions. *Front Microbiol* **11**: 1298.
814 **Parker JE, Holub EB, Frost LN, Falk A, Gunn ND, Daniels MJ. 1996.** Characterization of
815 eds1, a mutation in Arabidopsis suppressing resistance to Peronospora parasitica specified
816 by several different RPP genes. *Plant Cell* **8**(11): 2033-2046.
817 **Pruitt RN, Gust AA, Nurnberger T. 2021a.** Plant immunity unified. *Nat Plants* **7**(4): 382-
818 383.
819 **Pruitt RN, Locci F, Wanke F, Zhang L, Saile SC, Joe A, Karelina D, Hua C, Frohlich K,**
820 **Wan WL, et al. 2021b.** The EDS1-PAD4-ADR1 node mediates Arabidopsis pattern-
821 triggered immunity. *Nature* **598**(7881): 495-499.
822 **Quezada EH, Garcia GX, Arthikala MK, Melappa G, Lara M, Nanjareddy K. 2019.**
823 Cysteine-rich receptor-like kinase gene family identification in the phaseolus genome and
824 comparative analysis of their expression profiles specific to mycorrhizal and rhizobial
825 symbiosis. *Genes (Basel)* **10**(1).

826 **Rao S, Zhou Z, Miao P, Bi G, Hu M, Wu Y, Feng F, Zhang X, Zhou JM. 2018.** Roles of
827 receptor-like cytoplasmic kinase VII members in pattern-triggered immune signaling.
828 *Plant Physiol* **177**(4): 1679-1690.
829 **Schulze S, Yu L, Hua C, Zhang L, Kolb D, Weber H, Ehinger A, Saile SC, Stahl M, Franz-**
830 **Wachtel M, et al. 2022.** The Arabidopsis TIR-NBS-LRR protein CSA1 guards BAK1-
831 BIR3 homeostasis and mediates convergence of pattern- and effector-induced immune
832 responses. *Cell Host Microbe* **30**(12): 1717-1731 e1716.
833 **Schwessinger B, Roux M, Kadota Y, Ntoukakis V, Sklenar J, Jones A, Zipfel C. 2011.**
834 Phosphorylation-dependent differential regulation of plant growth, cell death, and innate
835 immunity by the regulatory receptor-like kinase BAK1. *PLoS Genet* **7**(4): e1002046.
836 **Smakowska-Luzan E, Mott GA, Parys K, Stegmann M, Howton TC, Layeghifard M,**
837 **Neuhold J, Lehner A, Kong J, Grunwald K, et al. 2018.** An extracellular network of
838 Arabidopsis leucine-rich repeat receptor kinases. *Nature* **553**(7688): 342-346.
839 **Sun X, Lapin D, Feehan JM, Stolze SC, Kramer K, Dongus JA, Rzemieniewski J,**
840 **Blanvillain-Baufume S, Harzen A, Bautor J, et al. 2021.** Pathogen effector recognition-
841 dependent association of NRG1 with EDS1 and SAG101 in TNL receptor immunity. *Nat*
842 *Commun* **12**(1): 3335.
843 **Swiderski MR, Birker D, Jones JD. 2009.** The TIR domain of TIR-NB-LRR resistance
844 proteins is a signaling domain involved in cell death induction. *Mol Plant Microbe Interact*
845 **22**(2): 157-165.
846 **Tang D, Wang G, Zhou JM. 2017.** Receptor kinases in plant-pathogen interactions: more than
847 pattern recognition. *Plant Cell* **29**(4): 618-637.
848 **Tian H, Wu Z, Chen S, Ao K, Huang W, Yaghmaiean H, Sun T, Xu F, Zhang Y, Wang S,**
849 **et al. 2021.** Activation of TIR signalling boosts pattern-triggered immunity. *Nature*
850 **598**(7881): 500-503.
851 **van Wersch S, Tian L, Hoy R, Li X. 2020.** Plant NLRs: The whistleblowers of plant immunity.
852 *Plant Commun* **1**(1): 100016.
853 **Wan WL, Zhang L, Pruitt R, Zaidem M, Brugman R, Ma X, Krol E, Perraki A, Kilian J,**
854 **Grossmann G, et al. 2019.** Comparing Arabidopsis receptor kinase and receptor protein-
855 mediated immune signaling reveals BIK1-dependent differences. *New Phytol* **221**(4):
856 2080-2095.
857 **Wang G, Ellendorff U, Kemp B, Mansfield JW, Forsyth A, Mitchell K, Bastas K, Liu CM,**
858 **Woods-Tor A, Zipfel C, et al. 2008.** A genome-wide functional investigation into the
859 roles of receptor-like proteins in Arabidopsis. *Plant Physiol* **147**(2): 503-517.

860 **Wang J, Chai J. 2020.** Structural insights into the plant immune receptors PRRs and NLRs.
861 *Plant Physiol* **182**(4): 1566-1581.
862 **Wang Y, Li X, Fan B, Zhu C, Chen Z. 2021.** Regulation and function of defense-related
863 callose deposition in plants. *Int J Mol Sci* **22**(5).
864 **Withers J, Dong X. 2017.** Post-translational regulation of plant immunity. *Curr Opin Plant*
865 *Biol* **38**: 124-132.
866 **Wu Y, Gao Y, Zhan Y, Kui H, Liu H, Yan L, Kemmerling B, Zhou JM, He K, Li J. 2020.**
867 Loss of the common immune coreceptor BAK1 leads to NLR-dependent cell death. *Proc*
868 *Natl Acad Sci U S A* **117**(43): 27044-27053.
869 **Xu B, Cheval C, Laohavisit A, Hocking B, Chiasson D, Olsson TSG, Shirasu K, Faulkner**
870 **C, Gilliham M. 2017.** A calmodulin-like protein regulates plasmodesmal closure during
871 bacterial immune responses. *New Phytol* **215**(1): 77-84.
872 **Yeh YH, Chang YH, Huang PY, Huang JB, Zimmerli L. 2015.** Enhanced Arabidopsis
873 pattern-triggered immunity by overexpression of cysteine-rich receptor-like kinases. *Front*
874 *Plant Sci* **6**: 322.
875 **Yip Delormel T, Boudsocq M. 2019.** Properties and functions of calcium-dependent protein
876 kinases and their relatives in Arabidopsis thaliana. *New Phytol* **224**(2): 585-604.
877 **Yu TY, Sun MK, Liang LK. 2021.** Receptors in the Induction of the Plant Innate Immunity.
878 *Mol Plant Microbe Interact* **34**(6): 587-601.
879 **Yuan M, Cai B, Xin XF. 2023.** Plant immune receptor pathways as a united front against
880 pathogens. *PLoS Pathog* **19**(2): e1011106.
881 **Yuan M, Jiang Z, Bi G, Nomura K, Liu M, Wang Y, Cai B, Zhou JM, He SY, Xin XF.**
882 **2021a.** Pattern-recognition receptors are required for NLR-mediated plant immunity.
883 *Nature* **592**(7852): 105-109.
884 **Yuan M, Ngou BPM, Ding P, Xin XF. 2021b.** PTI-ETI crosstalk: an integrative view of plant
885 immunity. *Curr Opin Plant Biol* **62**: 102030.
886 **Zhang W, Fraiture M, Kolb D, Loffelhardt B, Desaki Y, Boutrot FF, Tor M, Zipfel C,**
887 **Gust AA, Brunner F. 2013.** Arabidopsis receptor-like protein30 and receptor-like kinase
888 suppressor of BIR1-1/EVERSHED mediate innate immunity to necrotrophic fungi. *Plant*
889 *Cell* **25**(10): 4227-4241.
890 **Zhou JM, Zhang Y. 2020.** Plant immunity: danger perception and signaling. *Cell* **181**(5): 978-
891 989.
892 **Zhou N, Tootle TL, Tsui F, Klessig DF, Glazebrook J. 1998.** PAD4 functions upstream from
893 salicylic acid to control defense responses in Arabidopsis. *Plant Cell* **10**(6): 1021-1030.

894

895 **Figure legends**

896 **Figure 1. Transcriptional reprogramming associated to BAK1-INTERACTING**
897 **RECEPTOR-LIKE KINASE 1 (BIR1) induction in Arabidopsis.**

898 A) Morphology of representative BIR1 transgenic Arabidopsis plants (line 9, L9) under the
899 control of a dexamethasone (DEX)-inducible 35S promoter used for RNA-Seq experiments.
900 Samples were collected after 4 or 12 days of 30 µM DEX treatment. H_2O-treated plants were
901 used as controls. Relative BIR1 expression based on the number of Fragments Per Kilobase of
902 transcript sequence per Millions of base-pairs sequenced (FPKM) (top) and Western blot using
903 anti-mCherry antibody (bottom) in samples used for RNA-Seq. Significant differences between
904 DEX- and mock-treated samples were analyzed using two-way ANOVA followed by Sidak´s
905 multiple comparison test; ***, adjusted *p*-value < 0.001. B) Principal component analysis
906 (PCA) of RNA-Seq data. The PCA was performed using normalized RNA-Seq data of
907 differentially expressed genes (DEGs) between BIR1 L9 and wild-type (WT) plants after 4 and
908 12 days of DEX treatment (DeL9_vs DeWT_). Each biological replicate is represented in the
909 score plot. The variance explained by each component (%) is given in parentheses. The sample
910 (DeL9_12) with differential expression within the DEX-treated L9 group is indicated with
911 black arrows in (a) and (b). C) Number of up-or down-regulated transcripts, with a $|\log_2$ (Fold-
912 Change)$| \geq 1$ and adjusted *p*-value ≤ 0.01, in each pairwise comparison is indicated. D)
913 Scatterplot of selected gene ontology (GO) terms of DEGs. GO terms between WT and BIR1
914 L9 plants at 4 and 12 days after DEX-treatment (DeL9_ vs DeWT_) are shown. Dot size
915 represents the count of different genes and the color indicates significance of the term
916 enrichment. GO terms with adjusted *p*-value < 0.05 are significantly enriched. The kinase term
917 (indicated by an arrow) was exclusively assigned to BIR1 L9 plants. WT, wild-type Col-0; L9,
918 BIR1 L9 transgenic plants; De, DEX-treated plants; Mo, Mock-treated plants; _4, 4 days of
919 treatment; _12, 12 days of treatment.

920

921 **Figure 2. Effect of BAK1-INTERACTING RECEPTOR-LIKE KINASE 1 (BIR1)**
922 **induction on immune responses triggered by flg22 and nlp20 treatments.**

923 A) Over time production of reactive oxygen species (ROS) in dexamethasone (DEX)-treated
924 wild-type (WT) and BIR1 L6 and L9 transgenic plants after elicitation of Arabidopsis leaf disks
925 with 1 µM flg22 (left) or H_2O (right). Bars represent means ± SD of relative fluorescence units.
926 B) Ethylene accumulation in BIR1 L6 and L9 transgenic plants after treatment with H_2O

927 (mock), flg22 and nlp20 at 1 µM or 100 nM concentration as indicated. Bars represent average
928 values ± SD. Within each elicitor/mock treatment, differences between DEX-treated (DEX+)
929 and controls (DEX-) were analyzed by two-way ANOVA followed by Sidak´s multiple
930 comparison test. C) RT-qPCR analysis of the PTI-marker genes FLG22-INDUCED
931 RECEPTOR-LIKE KINASE 1 (FRK1) and PATHOGENESIS RELATED 1 (PR1) at 45 min
932 after treatment with H_2O (mock) or 1 µM flg22, and determined in DEX-treated (DEX+) versus
933 non-treated (DEX-) samples. D) Immunoprecipitation of mCherry-BIR1 fusion proteins,
934 indicated with an arrowhead, from samples of BIR1 L6 and L9 plants used in (A) and (B) (left),
935 and RT-qPCR analysis of BIR1 transcripts in DEX-treated (DEX+) samples of BIR1 L6 and
936 L9 plants used in (C) (right). In all cases, RT-qPCR values from biologically independent
937 samples were normalized to the CBP20 internal control, and related to H_2O (mock)-treated
938 plants, set to a value of 1. Data are means ± SD analyzed by Kruskal-Wallis test; *, adjusted *p*-
939 value <0.05. Experiments were repeated three times with similar results.

940

941 **Figure 3. BAK1-INTERACTING RECEPTOR-LIKE KINASE 1 (BIR1) induction**
942 **inhibits flg22- and poly(I:C)-triggered callose accumulation at plasmodesmata (PD)**.

943 Callose spots at PD were visualized upon aniline blue staining of epidermal cells in response to
944 bacterial flg22 (A) or poly(I:C) (B) in BIR1 L9 transgenic Arabidopsis plants. Plants were
945 previously treated with 30 µM dexamethasone (DEX) to elicit BIR1 expression. Mock-treated
946 plants were used as non BIR1-expressing controls (top panels). Photographs were taken 30
947 minutes after treatment with H_2O (control) or 1 µM flg22 or 50 ng/µl of poly(I:C). BIR1-
948 mCherry fluorescence in DEX-treated BIR1 L9 plants was confirmed within the same images.
949 Inlays show enlargements of the areas within the dashed boxes. Scale bar, 10 µm. C) Relative
950 PD callose content in flg22/poly(I:C)-treated and H_2O (control)-treated leaves from BIR1 L9
951 plants previously treated with or without DEX as indicated. Callose content at PD in DEX-
952 treated wild-type (WT) plants in response to poly (I:C) is shown. D) flg22/poly(I:C)-induced
953 callose content at PD in the *sobir1-12* and *bir1-1 sobir1-1* mutants. H_2O-treated controls and
954 callose deposition at PD from WT Col-0 leaves are shown as controls. In all cases, black dots
955 represent the mean values of callose intensities in individual PD (>100) measured in three leaf
956 discs taken from at least three independent biological replicates per each treatment. Significant
957 differences between samples were analyzed by Kruskal-Wallis test or by one-way ANOVA
958 followed by Tukey's multiple comparison test; ****, adjusted *p*-value <0.0001, ***, <0.001,
959 **, <0.01. Experiments were repeated twice with similar results.

960

961 **Figure 4. BAK1-INTERACTING RECEPTOR-LIKE KINASE 1 (BIR1) overexpression**
962 **leads to the transcriptional activation of pattern-triggered immunity (PTI)-associated co-**
963 **receptors and effector-triggered immunity (ETI) regulators.**

964 A) Validation of the RNA-Seq results. Expression of selected BIR1-responsive differentially
965 expressed genes (DEGs) after 12 days of dexamethasone (DEX) treatment based on fold-change
966 values ($\log_2$ DeL9_12/DeWT_12 and $\log_2$ DeL9_12/MoL9_12 as indicated) was confirmed by
967 RT-qPCR. Values from biologically independent samples were normalized to the CBP20
968 internal control, and related to untreated (DEX-) plants, set to a value of 1. Data are mean ± SD
969 analyzed by Mann-Whitney test; *, p <0.05. B) Relative expression of selected PTI/ETI-related
970 genes based on the number of Fragments Per Kilobase of transcript sequence per Millions of
971 base-pairs sequenced (FPKM) in each of the three independent samples per condition used for
972 RNA-Seq. Actin expression is shown as control. Note that the expression levels of each
973 individual replicate within the DEX-treated BIR1 L9_12 group mirror the abundance of BIR1
974 transcripts in each replicate. Significant differences between mock-treated and DEX-treated
975 samples were analyzed using two-way ANOVA followed by Sidak´s multiple comparison test;
976 ****, adjusted p-value < 0.0001, *** < 0.001, **< 0.01. WT, wild-type Col-0; L9, BIR1 L9
977 transgenics; _4d, 4 days of treatment; _12d, 12 days of treatment. C) Western blot analysis of
978 SUPPRESSOR OF BIR1-1 (SOBIR1) and PATHOGENESIS RELATED 1 (PR1) using
979 specific antibodies in two independent sets of BIR1 L9 samples. Plants were mock-treated (-)
980 or DEX-treated (+) for 12 days. The presence (+) or absence (-) of morphological phenotypes
981 (Ph) in each sample is indicated. Protein loading control by Ponceau S is shown.

982

983 **Figure 5. Phenotypes caused by BAK1-INTERACTING RECEPTOR-LIKE KINASE 1**
984 **(BIR1) overexpression are partially rescued in *sobir1-12* mutants, but not in a *bak1-5***
985 **mutant.**

986 A) Morphology of transgenic *sobir1-12* BIR1 L6 and *bak1*-5 BIR1 L10 mutant plants
987 expressing BIR1 under the control of a dexamethasone (DEX)-inducible 35S promoter.
988 Transgenic BIR1 L9 plants in the wild-type (WT) Col-0 background are shown as a reference.
989 Plants were grown for three weeks on soil and treated with 30 µM dexamethasone (DEX) to
990 induce BIR1 transcription or mock-treated with H_2O. Non-transgenic WT Col-0 plants are
991 shown as controls. Plants were photographed after 12 days of the first DEX/ H_2O application.

992 Images from independent transgenic lines are shown in Fig. S7. RT-qPCR analysis of *BIR1*
993 transcripts in BIR1 L9 plants are shown. B) RT-qPCR analysis of BIR1 and ENHANCED
994 DISEASE SUSCEPTIBILITY 1 (EDS1) transcripts in *sobir1-12* BIR1 L6 and *bak1*-5 BIR1
995 L10 plants. C) Western blot analysis of BIR1 and EDS1 proteins with specific antibodies in
996 WT BIR1 L9 and two independent lines of *sobir1-12* BIR1 (L6, L8) and *bak1*-5 BIR1 (L4,
997 L10). Plants were mock-treated (-) or DEX-treated (+) for 12 days as indicated. The presence
998 (+) or absence (-) of morphological phenotypes (Ph) in each sample is indicated. Protein loading
999 control by Ponceau S is shown. RT-qPCR analysis of the PTI-marker genes RESPIRATORY
1000 BURST OXIDASE HOMOLOG PROTEIN D (RBOHD), FLG22-INDUCED RECEPTOR-
1001 LIKE KINASE 1 (FRK1) or WRKY DNA-BINDING PROTEIN 29 (WRKY29) in *sobir1-12*
1002 BIR1 L6 (D) and *bak1*-5 BIR1 L10 (E) plants. RT-qPCR analysis of representative marker
1003 genes of the salicylic acid PATHOGENESIS RELATED 1 (PR1), jasmonic acid PLANT
1004 DEFENSIN 1.2 (PDF1.2), ethylene PR4 and camalexin [PHYTOALEXIN DEFICIENT 3
1005 (PAD3), CYTOCHROME P450 MONOOXYGENASE 79B2 (CYP79B2)] pathways in
1006 *sobir1-12* BIR1 L6 (F) and *bak1*-5 BIR1 L10 (G) plants. In all cases, the same set of replicates
1007 from each genotype was used to measure all the genes shown in the graphs. Transcript
1008 accumulation was determined in mock-treated (DEX-) versus DEX-treated (DEX+) after 12
1009 days of treatment. Values from biologically independent samples were normalized to the
1010 CBP20 internal control, and related to mock-treated plants, set to a value of 1. Data are mean ±
1011 SD analyzed by Mann-Whitney test; *, p <0.05. Experiments were repeated at least twice with
1012 similar results.

1013

1014 **Figure 6. Phenotypes caused by BAK1-INTERACTING RECEPTOR-LIKE KINASE 1**
1015 **(BIR1) overexpression are partially rescued in *eds1-2* mutants, but not in a *pad4-1* mutant.**

1016 A) Morphology of transgenic *eds1-2* BIR1 L1b and *pad4-1* BIR1 L0 mutant plants expressing
1017 BIR1 under the control of a dexamethasone (DEX)-inducible 35S promoter. Plants were grown
1018 for three weeks on soil and treated with 30 µM DEX to induce BIR1 transcription or mock-
1019 treated with H_2O. Plants were photographed after 12 days of the first DEX/ H_2O application.
1020 Images from independent transgenic lines are shown in Fig. S7. RT-qPCR analysis of BIR1
1021 transcript in *eds1-2* BIR1 L1b and *pad4-1* BIR1 L0 mutant lines are shown. RT-qPCR analysis
1022 of the PTI-marker genes RESPIRATORY BURST OXIDASE HOMOLOG PROTEIN D
1023 (RBOHD) and FLG22-INDUCED RECEPTOR-LIKE KINASE 1 (FRK1) in *eds1-2* BIR1 L1b
1024 (B) and *pad4-1* BIR1 L0 (C) plants. RT-qPCR analysis of representative marker genes of the

1025 salicylic acid PATHOGENESIS RELATED 1 (PR1), jasmonic acid PLANT DEFENSIN 1.2
1026 (PDF1.2), ethylene PR4 and camalexin [PHYTOALEXIN DEFICIENT 3 (PAD3),
1027 CYTOCHROME P450 MONOOXYGENASE 79B2 (CYP79B2)] pathways in *eds1-2* BIR1
1028 L1b (D) and *pad4-1* BIR1 L0 (E) plants. In all cases, the same set of replicates from each
1029 genotype was used to measure all the genes shown in the graphs. Transcript accumulation was
1030 determined in mock-treated (DEX-) versus DEX-treated (DEX+) after 12 days of treatment.
1031 Values from biologically independent samples were normalized to the CBP20 internal control,
1032 and related to mock-treated plants, set to a value of 1. Data are mean ± SD analyzed by Mann-
1033 Whitney test; *, p <0.05. Experiments were repeated at least twice with similar results.

1034

1035 **Figure 7. Phenotypes caused by BAK1-INTERACTING RECEPTOR-LIKE KINASE 1**
1036 **(BIR1) overexpression are independent of salicylic acid (SA)-mediated signaling**
1037 **pathways.**

1038 A) Morphology of transgenic *sid2-2* BIR1 (L5) and *eds5-3* BIR1 (L10) mutant plants
1039 expressing BIR1 under the control of a dexamethasone (DEX)-inducible 35S promoter. Plants
1040 were grown for three weeks on soil and treated with 30 µM DEX to induce BIR1 transcription
1041 or mock-treated with H_2O. Plants were photographed after 12 days of the first DEX/ H_2O
1042 application. Images from independent transgenic lines are shown in Fig. S7a, b. RT-qPCR
1043 analysis of BIR1 and representative marker genes of the jasmonic acid PLANT DEFENSIN 1.2
1044 (PDF1.2) and camalexin [PHYTOALEXIN DEFICIENT 3 (PAD3), CYTOCHROME P450
1045 MONOOXYGENASE 79B2 (CYP79B2)] pathways in *sid2-2* BIR1 (L5) (B) and *eds5-3* BIR1
1046 (L10) (C) mutant lines. In all cases, the same set of replicates from each genotype was used to
1047 measure all the genes shown in the graphs. Transcript accumulation was determined in mock-
1048 treated (DEX-) versus DEX-treated (DEX+) after 12 days of treatment. Values from
1049 biologically independent samples were normalized to the *CBP20* internal control, and related
1050 to mock-treated plants, set to a value of 1. Data are mean ± SD analyzed by Mann-Whitney test;
1051 *, p <0.05. Experiments were repeated at least twice with similar results. D) Tentative working
1052 model for BIR1 homeostasis. SA-mediated transcription of BIR1 is regulated by RNA-directed
1053 DNA methylation (RdDM) and post-transcriptional RNA silencing (PTGS) (Guzman-Benito *et*
1054 *al.*, 2019). In these conditions, BIR1 induction interferes with PTI gene expression and PD
1055 callose deposition triggered by various elicitors (flg22, nlp20, dsRNA). Loss of BIR1 regulation
1056 leads to constitutive BIR1 induction and ultimately BIR1 overexpression at levels that cause
1057 SA-independent up-regulation of immune and hormone genes. BIR1 overexpression is sensed

1058 by one or several TNLs, of which CSA1 is a plausible candidate, to promote PAD4-independent
1059 ETI-type cell death that requires EDS1 and SOBIR1.

1060

1061

1062 **Supporting information**

1063 **Figure S1. Transcriptomic profiling of BAK1-INTERACTING RECEPTOR-LIKE**
1064 **KINASE 1 (BIR1) expressing transgenic lines.**

1065 A) Principal component analysis (PCA) of RNA-Seq data. The PCA was performed using
1066 normalized RNA-Seq data of differentially expressed genes (DEGs) between dexamethasone
1067 (DEX)-treated and mock-treated transgenic BIR1 L9 plants after 4 and 12 days of treatment
1068 (DeL9_vs MoL9_). Each biological replicate is represented in the score plot. The variance
1069 explained by each component (%) is given in parentheses. B) Number of up-or down-regulated
1070 transcripts, with a $|\log_2$ (Fold-Change)$| \geq 1$ and adjusted *p*-value ≤ 0.05, in each pairwise
1071 comparison as indicated. C) Volcano plots showing the distribution of DEGs (adjusted *p*-value
1072 ≤ 0.05). The x-axis shows the fold change in gene expression between samples, and y-axis
1073 shows the statistical significance of the differences. Significantly up- and down-regulated genes
1074 are highlighted in red and green, respectively. Genes that are not differentially regulated are in
1075 blue. D) Scatterplot of selected gene ontology (GO) terms of DEGs. GO terms between wild-
1076 type (WT) and BIR1 L9 plants at 4 and 12 days after DEX-treatment (DeL9_ vs MoL9_) are
1077 shown. Dot size represents the count of different genes and the color indicates significance of
1078 the term enrichment. GO terms with adjusted *p*-value < 0.05 are significantly enriched. The
1079 kinase term (indicated by an arrow) was exclusively assigned to BIR1 L9 plants. WT, wild-
1080 type Col-0; L9, BIR1 L9 transgenic plants; De, DEX-treated plants; Mo, Mock-treated plants;
1081 _4, 4 days of treatment; _12, 12 days of treatment.

1082

1083 **Figure S2. Transcriptomic profiling of dexamethasone (DEX)-treated wild-type Col-0**
1084 **plants.**

1085 A) Morphology of representative wild-type (WT) Arabidopsis plants used for RNA-Seq
1086 experiments. Samples were collected after 4 or 12 days of 30 μM DEX treatment and subjected
1087 to RNA sequencing. H_2O-treated plants were used as controls. Note that application of DEX
1088 has a negative effect on plant growth as deduced by the significant reduction of rosette size
1089 after 12 days of DEX treatment relative to the non-treated controls. Box and whisker plot
1090 showing 5-95 percentile was analyzed by Mann-Whitney test; ****, $p < 0.0001$. B) Volcano
1091 plots showing the distribution of differentially expressed genes (DEGs) (adjusted *p*-value $\leq$
1092 0.05). The x-axis shows the gene fold change, and y-axis plots the statistical significance (*p*-
1093 value) of the differences. Significantly up- and down-regulated genes are highlighted in red and

green, respectively. Genes that are not differentially regulated are in blue. C) Principal component analysis (PCA) of RNA-Seq data. The PCA was performed using normalized RNA-Seq data of DEGs between DEX-treated and mock-treated WT plants after 4 and 12 days of treatment (DeWT_vs MoWT_). Each biological replicate is represented in the score plot. The variance explained by each component (%) is given in parentheses. D) Scatterplot of selected gene ontology (GO) terms of DEGs. GO terms between DEX-treated and mock-treated WT plants at 4 and 12 days of treatment (DeL9_ vs MoL9_) are shown. Dot size represents the count of different genes and the color indicates significance of the term enrichment. GO terms with adjusted *p*-value < 0.05 are significantly enriched. WT, wild-type Col-0; De, DEX-treated plants; Mo, Mock-treated plants; _4, 4 days of treatment; _12, 12 days of treatment.

Figure S3. Enrichment analysis of Kyoto Encyclopedia of Genes and Genomes (KEGG) pathways using RNA-Seq data.

Scatterplot of selected Kyoto Encyclopedia of Genes and Genomes (KEGG) pathways. Dot size represents the count of different genes and the color indicates significance of the term enrichment. Terms with adjusted *p*-value < 0.05 are significantly enriched. WT, wild-type Col-0; De, DEX-treated plants; Mo, Mock-treated plants; _4, 4 days of treatment; _12, 12 days of treatment.

Figure S4. Differential expression of receptor-like protein (RLP)-coding genes in BAK1-INTERACTING RECEPTOR-LIKE KINASE 1 (BIR1) overexpressing plants.

A) Relative expression levels of selected RLP-coding genes based on the number of Fragments Per Kilobase of transcript sequence per Millions of base-pairs sequenced (FPKM) in each of the three independent samples per condition used for RNA-Seq. Significant differences between dexamethasone (DEX)- and mock-treated samples were analyzed using two-way ANOVA followed by Sidak´s multiple comparison test; ***, adjusted *p*-value < 0.001, **< 0.01. Note that the expression levels of each individual replicate within the DEX-treated BIR1 L9_12 group mirror the abundance of BIR1 transcripts in each replicate. B) Differential expression of selected BIR1-responsive RLP-coding genes based on $\log_2$ fold-change in the indicated pairwise comparisons. WT, wild-type Col-0; L9, BIR1 L9 transgenics; De, DEX-treated plants; Mo, mock-treated plants: _4d, 4 days of treatment; _12d, 12 days of treatment.

1126 **Figure S5. Differential expression of cysteine-rich receptor-like kinase (CRK)-coding**
1127 **genes in BAK1-INTERACTING RECEPTOR-LIKE KINASE 1 (BIR1) overexpressing**
1128 **plants.**

1129 A) Relative expression levels of selected CRK-coding genes based on the number of Fragments
1130 Per Kilobase of transcript sequence per Millions of base-pairs sequenced (FPKM) in each of
1131 the three independent samples per condition used for RNA-Seq. Significant differences
1132 between dexamethasone (DEX)- and mock-treated samples were analyzed using two-way
1133 ANOVA followed by Sidak´s multiple comparison test; ***, adjusted *p*-value < 0.001, **<
1134 0.01. Note that the expression levels of each individual replicate within the DEX-treated BIR1
1135 L9_12 group mirror the abundance of BIR1 transcripts in each replicate. B) Differential
1136 expression of selected BIR1-responsive CRK-coding genes based on $\log_2$ fold-change in the
1137 indicated pairwise comparisons. WT, wild-type Col-0; L9, BIR1 L9 transgenics; De, DEX-
1138 treated plants; Mo, mock-treated plants: _4d, 4 days of treatment; _12d, 12 days of treatment.

1139

1140 **Figure S6. Differential expression of cell-surface pattern recognition receptors (PRR) and**
1141 **calcium-dependent protein kinases (CPK)-encoding genes in BAK1-INTERACTING**
1142 **RECEPTOR-LIKE KINASE 1 (BIR1) overexpressing plants.**

1143 Relative expression levels of selected PRR- (A) and CPK-coding genes (B) based on the
1144 number of Fragments Per Kilobase of transcript sequence per Millions of base-pairs sequenced
1145 (FPKM) in each of the three independent samples per condition used for RNA-Seq. Significant
1146 differences between dexamethasone (DEX)- and mock-treated samples were analyzed using
1147 two-way ANOVA followed by Sidak´s multiple comparison test; ***, adjusted *p*-value < 0.001,
1148 **< 0.01, *< 0.05. WT, wild-type Col-0; L9, BIR1 L9 transgenics; De, DEX-treated plants;
1149 Mo, mock-treated plants: _4d, 4 days of treatment; _12d, 12 days of treatment.

1150

1151 **Figure S7. Morphological and growth defects in BAK1-INTERACTING RECEPTOR-**
1152 **LIKE KINASE 1 (BIR1) overexpressing plants of different immune mutant genetic**
1153 **backgrounds.**

1154 A) Morphology of transgenic *sobir1-12* BIR1 L8, *bak1-5* BIR1 L4, *eds1*-2 BIR1 L2, *pad4-1*
1155 BIR1 L12b and *eds5-3* BIR1 L12 mutant plants from independent lines expressing BIR1 under
1156 the control of a dexamethasone (DEX)-inducible 35S promoter. Plants were grown for three
1157 weeks on soil and treated with 30 µM DEX to activate BIR1 transcription or mock-treated with

1158 H_2O. Plants were photographed after 12 days of the first DEX/ H_2O application. B) Morphology
1159 and BIR1 expression levels of DEX- and mock-treated *sobir1-12* BIR1 (L6, L8) and *bak1-5*
1160 BIR1 (L4, L10) plants as observed in different biological replicates of the experiment. qRT-
1161 PCR analysis showed comparable BIR1 transcript levels in both genotypes. Each sample
1162 consisted of RNA pooled from six different plants. C) RT-qPCR analysis of the PTI-marker
1163 WRKY DNA-BINDING PROTEIN 29 (WRKY29) gene in *sobir1-12* BIR1 L6 and *pad4*-1
1164 BIR1 L10 mutant backgrounds. In all cases, transcript accumulation was determined in DEX-
1165 treated (DEX+) versus mock-treated (DEX-) after 12 days of treatment. Values from
1166 biologically independent samples were normalized to the CBP20 internal control, and related
1167 to mock-treated plants, set to a value of 1. Data are mean ± SD analyzed by Mann-Whitney test;
1168 *, $p < 0.05$. D) Rosette size (diameter) in wild-type (WT) and BIR1 overexpressing ETI/PTI
1169 mutants after 12 days of DEX treatment relative to the non-treated controls. Box and whisker
1170 plots showing 5-95 percentile were analyzed by Mann-Whitney test; ****, $p < 0.0001$. Note that
1171 rosette size is largely influenced by the effect of DEX on plant development as shown for WT
1172 Col-0 plant in this study.

1173

1174 **Table S1. List of primers**

1175 **Table S2. List of expressed genes**

1176 Values represent the total read counts/ Fragments Per Kilobase of transcript sequence per
1177 Millions of base-pairs sequenced (FRKM) values of each biological replicate (a,b,c) per
1178 condition and their corresponding row mean values. De (DEX-treated plants), Mo (Mock-
1179 treated plants), WT (wild-type plants), L9 (BIR1 L9 transgenic plants), _4 (4 days of treatment),
1180 _12 (12 days of treatment).

1181

1182 **Table S3. List of differentially expressed genes (DEG. padjust value < 0.05)**

1183 Values represent the mean Fragments Per Kilobase of transcript sequence per Millions of base-
1184 pairs sequenced (FPKM) values from three biological replicates per condition. De (DEX-
1185 treated plants), Mo (Mock-treated plants), WT (wild-type plants), L9 (BIR1 L9 transgenic
1186 plants), _4 (4 days of treatment), _12 (12 days of treatment).

1187

1188 **Table S4. List of differentially expressed genes (DEG. |Log2fold change > 1| padjust value**
1189 **< 0.01)**

1190 Values represent the mean Fragments Per Kilobase of transcript sequence per Millions of base-
1191 pairs sequenced (FPKM) values from three biological replicates per condition. De (DEX-
1192 treated plants), Mo (Mock-treated plants), WT (wild-type plants), L9 (BIR1 L9 transgenic
1193 plants), _4 (4 days of treatment), _12 (12 days of treatment).

1194

1195 **Table S5. Enrichment analysis of Gene Ontology (GO) terms**

1196 CC (cellular component), BP (biological process) and MF (molecular function). Gene Ratio is
1197 the ratio of DEGs to all genes for this GO term. Bg Ratio is the ratio of all genes concerning
1198 this GO term to all genes in background GO database. Count is the number of differentially
1199 expressed genes concerning this GO term. Adjusted p-value < 0.05 means significant
1200 enrichment. De (DEX-treated plants), Mo (Mock-treated plants), WT (wild-type plants), L9
1201 (BIR1 L9 transgenic plants), _4 (4 days of treatment), _12 (12 days of treatment).

1202

1203 **Table S6. Kyoto Encyclopedia of Genes and Genomes (KEGG) pathway enrichment**
1204 **analysis**

1205 Gene Ratio is the ratio of DEGs to all genes for this pathway. Bg Ratio is the ratio of all genes
1206 concerning this KEGG term to all genes in background KEGG database. Count is the number
1207 of differentially expressed genes concerning this term. Adjusted p-value < 0.05 means
1208 significant enrichment. De (DEX-treated plants), Mo (Mock-treated plants), WT (wild-type
1209 plants), L9 (BIR1 L9 transgenic plants), _4 (4 days of treatment), _12 (12 days of treatment).

1210

1211 **Table S7. List of differentially expressed genes (DEG. padjust value < 0.05) within**
1212 **functional categories**

1213 Values represent the mean Fragments Per Kilobase of transcript sequence per Millions of base-
1214 pairs sequenced (FPKM) values from three biological replicates per condition. De (DEX-
1215 treated plants), Mo (Mock-treated plants), WT (wild-type plants), L9 (BIR1 L9 transgenic
1216 plants), _4 (4 days of treatment), _12 (12 days of treatment).

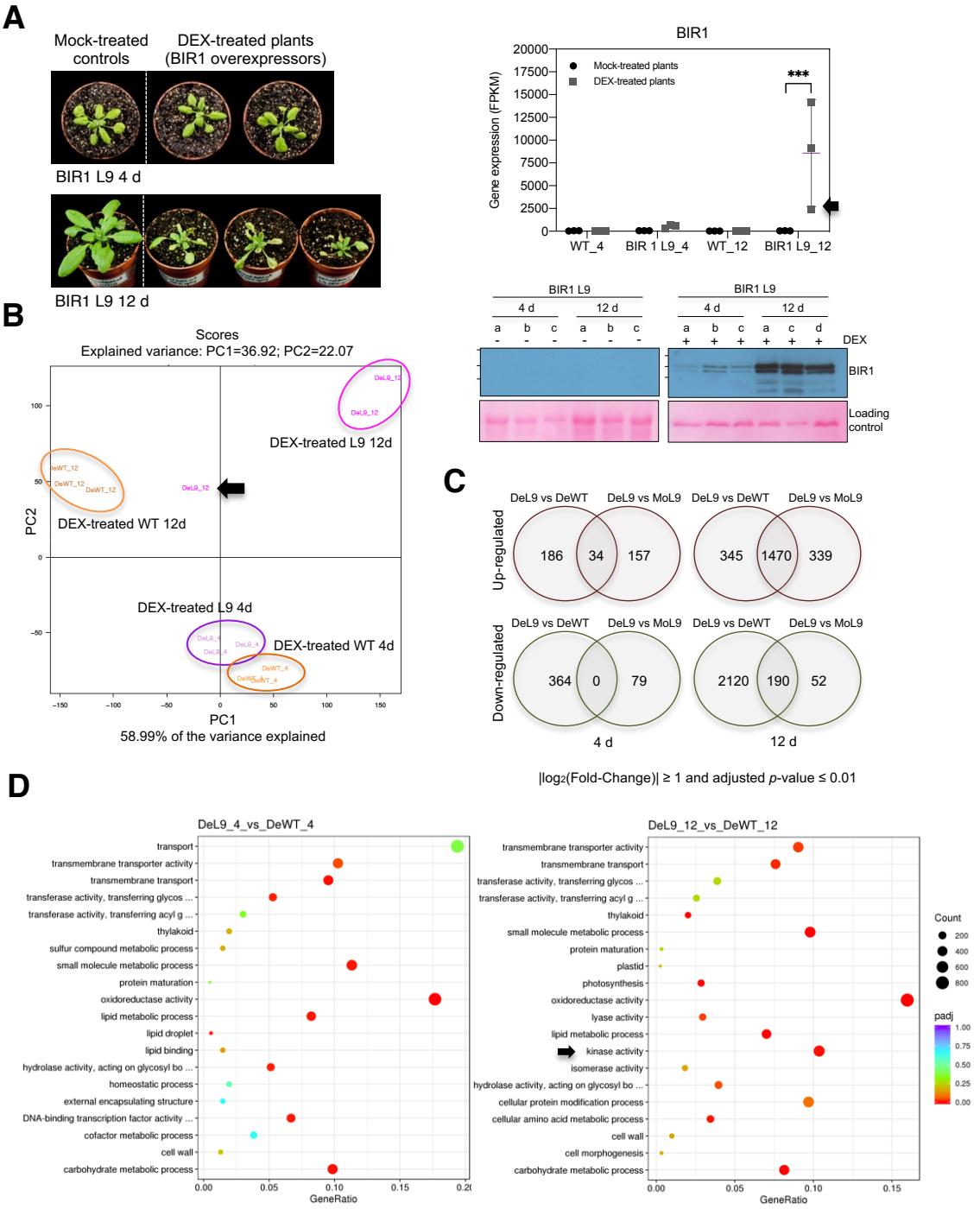

Figure 1. Transcriptional reprogramming associated to BAK1-INTERACTING RECEPTOR-LIKE KINASE 1 (BIR1) induction in Arabidopsis.
A) Morphology of representative BIR1 transgenic Arabidopsis plants (line 9, L9) under the control of a dexamethasone (DEX)-inducible 35S promoter used for RNA-Seq experiments. Samples were collected after 4 or 12 days of 30 µM DEX treatment. H_2O-treated plants were used as controls. Relative BIR1 expression based on the number of Fragments Per Kilobase of transcript sequence per Millions of base-pairs sequenced (FPKM) (top) and Western blot using anti-mCherry antibody (bottom) in samples used for RNA-Seq. Significant differences between DEX- and mock-treated samples were analyzed using two-way ANOVA followed by Sidak´s multiple comparison test; ***, adjusted *p*-value < 0.001. B) Principal component analysis (PCA) of RNA-Seq data. The PCA was performed using normalized RNA-Seq data of differentially expressed genes (DEGs) between BIR1 L9 and wild-type (WT) plants after 4 and 12 days of DEX treatment (DeL9_vs DeWT_). Each biological replicate is represented in the score plot. The variance explained by each component (%) is given in parentheses. The sample (DeL9_12) with differential expression within the DEX-treated L9 group is indicated with black arrows in (a) and (b). C) Number of up-or down-regulated transcripts, with a $|\log_2$ (Fold-Change)$| \geq 1$ and adjusted *p*-value ≤ 0.01, in each pairwise comparison is indicated. D) Scatterplot of selected gene ontology (GO) terms of DEGs. GO terms between WT and BIR1 L9 plants at 4 and 12 days after DEX-treatment (DeL9_ vs DeWT_) are shown. Dot size represents the count of different genes and the color indicates significance of the term enrichment. GO terms with adjusted *p*-value < 0.05 are significantly enriched. The kinase term (indicated by an arrow) was exclusively assigned to BIR1 L9 plants. WT, wild-type Col-0; L9, BIR1 L9 transgenic plants; De, DEX-treated plants; Mo, Mock-treated plants; _4, 4 days of treatment; _12, 12 days of treatment.

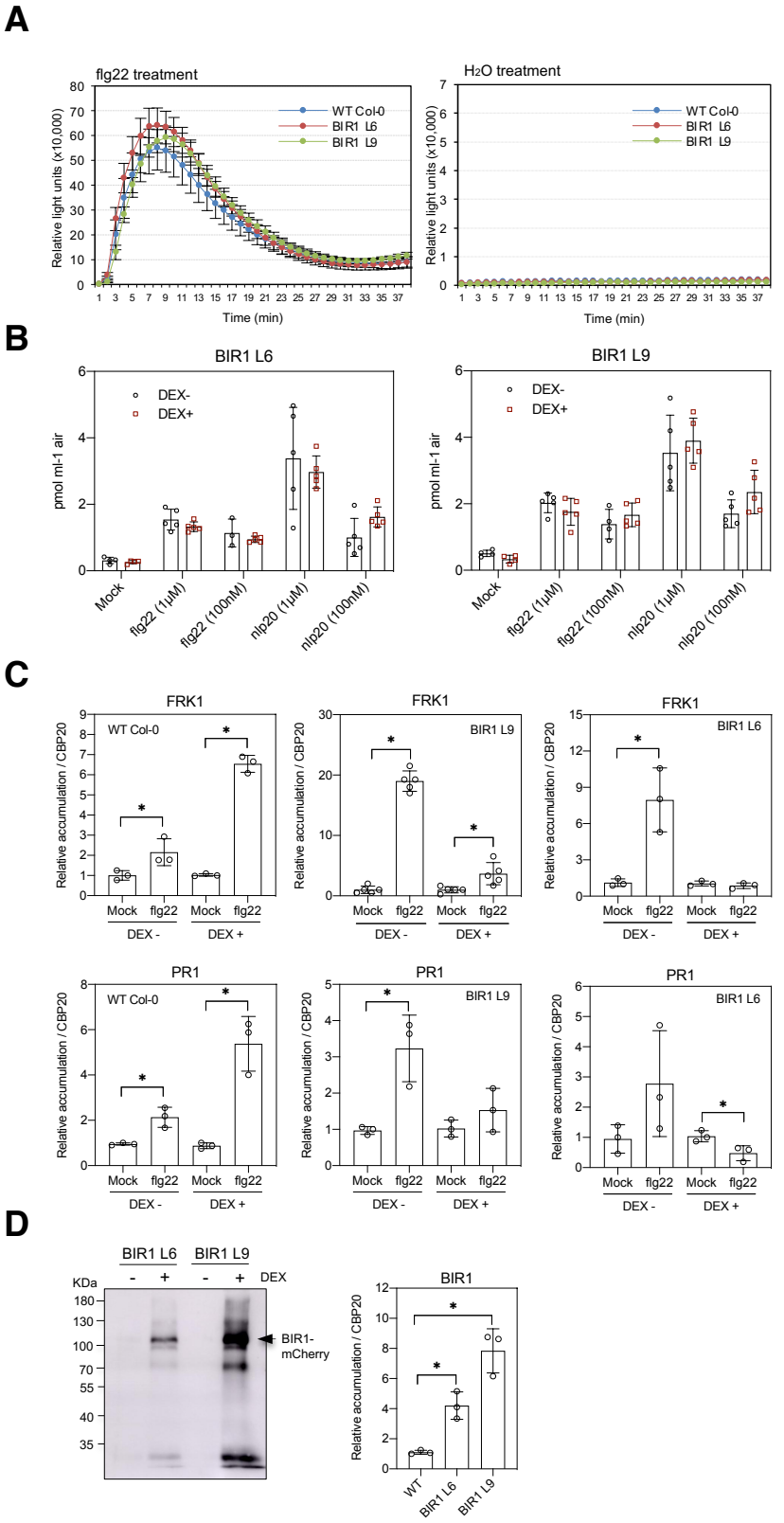

Figure 2. Effect of BAK1-INTERACTING RECEPTOR-LIKE KINASE 1 (BIR1) induction on immune responses triggered by flg22 and nlp20 treatments.

A) Over time production of reactive oxygen species (ROS) in dexamethasone (DEX)-treated wild-type (WT) and BIR1 L6 and L9 transgenic plants after elicitation of Arabidopsis leaf disks with 1 µM flg22 (left) or H_2O (right). Bars represent means ± SD of relative fluorescence units. B) Ethylene accumulation in BIR1 L6 and L9 transgenic plants after treatment with H_2O (mock), flg22 and nlp20 at 1 µM or 100 nM concentration as indicated. Bars represent average values ± SD. Within each elicitor/mock treatment, differences between DEX-treated (DEX+) and controls (DEX-) were analyzed by two-way ANOVA followed by Sidak´s multiple comparison test. C) RT-qPCR analysis of the PTI-marker genes FLG22-INDUCED RECEPTOR-LIKE KINASE 1 (FRK1) and PATHOGENESIS RELATED 1 (PR1) at 45 min after treatment with H_2O (mock) or 1 µM flg22, and determined in DEX-treated (DEX+) versus non-treated (DEX-) samples. D) Immunoprecipitation of mCherry-BIR1 fusion proteins, indicated with an arrowhead, from samples of BIR1 L6 and L9 plants used in (A) and (B) (left), and RT-qPCR analysis of BIR1 transcripts in DEX-treated (DEX+) samples of BIR1 L6 and L9 plants used in (C) (right). In all cases, RT-qPCR values from biologically independent samples were normalized to the CBP20 internal control, and related to H_2O (mock)-treated plants, set to a value of 1. Data are means ± SD analyzed by Kruskal-Wallis test; *, adjusted *p*-value <0.05. Experiments were repeated three times with similar results.

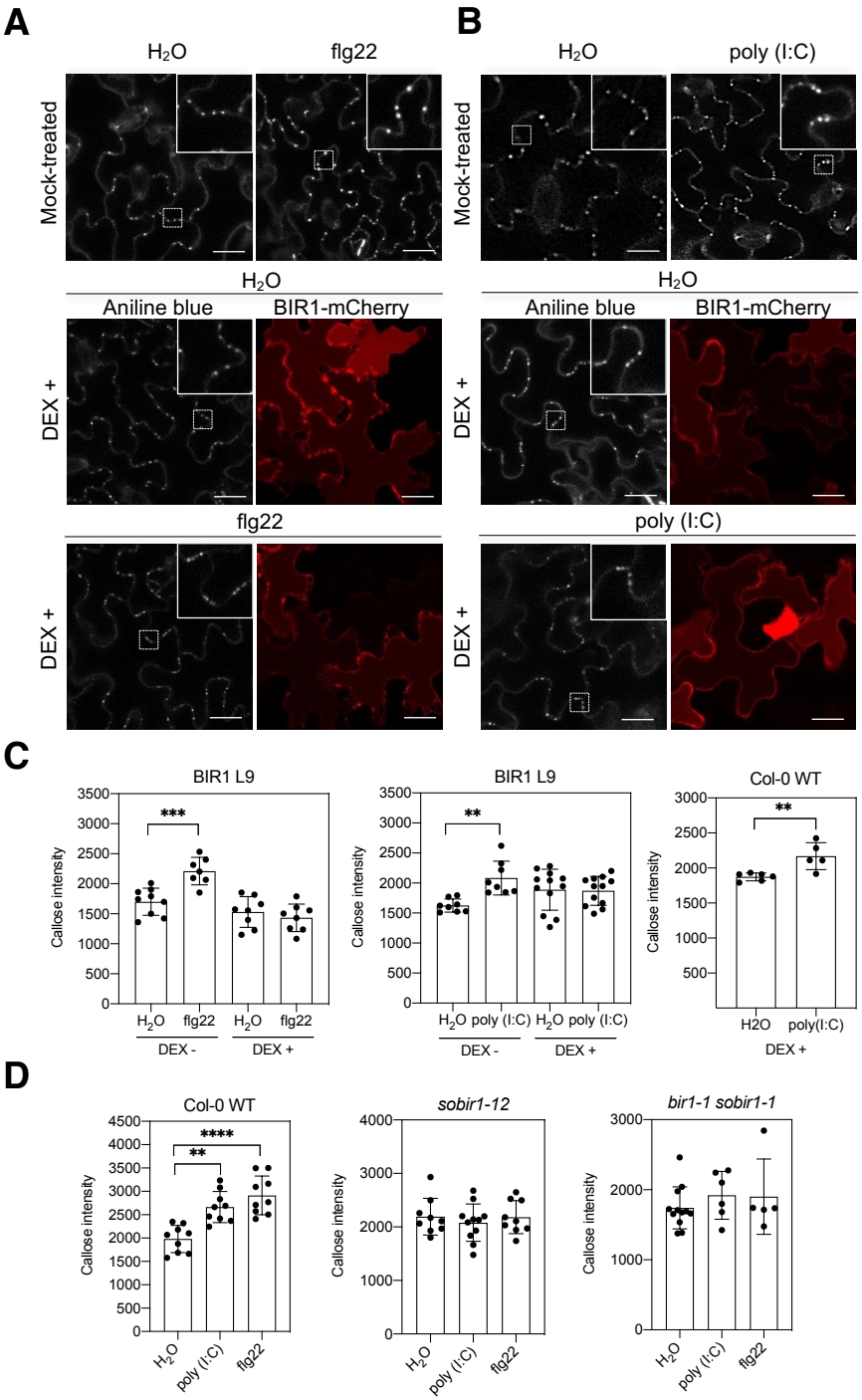

Figure 3. BAK1-INTERACTING RECEPTOR-LIKE KINASE 1 (BIR1) induction inhibits flg22- and poly(I:C)-triggered callose accumulation at plasmodesmata (PD).

Callose spots at PD were visualized upon aniline blue staining of epidermal cells in response to bacterial flg22 (A) or poly(I:C) (B) in BIR1 L9 transgenic Arabidopsis plants. Plants were previously treated with 30 µM dexamethasone (DEX) to elicit BIR1 expression. Mock-treated plants were used as non BIR1-expressing controls (top panels). Photographs were taken 30 minutes after treatment with H_2O (control) or 1 µM flg22 or 50 ng/µl of poly(I:C). BIR1-mCherry fluorescence in DEX-treated BIR1 L9 plants was confirmed within the same images. Inlays show enlargements of the areas within the dashed boxes. Scale bar, 10 µm. C) Relative PD callose content in flg22/poly(I:C)-treated and H_2O (control)-treated leaves from BIR1 L9 plants previously treated with or without DEX as indicated. Callose content at PD in DEX-treated wild-type (WT) plants in response to poly (I:C) is shown. D) flg22/poly(I:C)-induced callose content at PD in the *sobir1-12* and *bir1-1 sobir1-1* mutants. H_2O-treated controls and callose deposition at PD from WT Col-0 leaves are shown as controls. In all cases, black dots represent the mean values of callose intensities in individual PD (>100) measured in three leaf discs taken from at least three independent biological replicates per each treatment. Significant differences between samples were analyzed by Kruskal-Wallis test or by one-way ANOVA followed by Tukey's multiple comparison test; ****, adjusted *p*-value <0.0001, ***, <0.001, **, <0.01. Experiments were repeated twice with similar results.

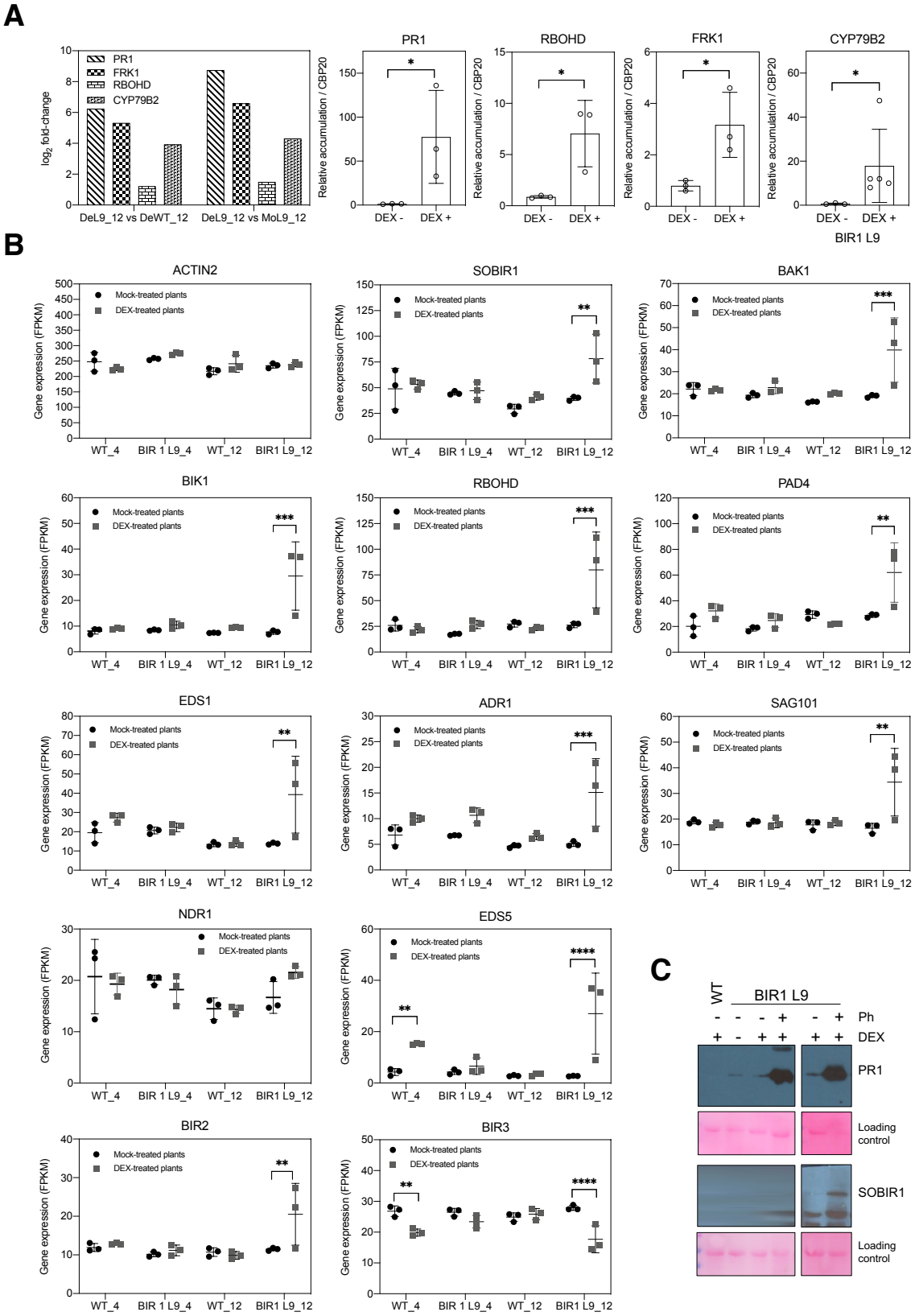

Figure 4. BAK1-INTERACTING RECEPTOR-LIKE KINASE 1 (BIR1) overexpression leads to the transcriptional activation of pattern-triggered immunity (PTI)-associated co-receptors and effector-triggered immunity (ETI) regulators.

A) Validation of the RNA-Seq results. Expression of selected BIR1-responsive differentially expressed genes (DEGs) after 12 days of dexamethasone (DEX) treatment based on fold-change values (log_2 DeL9_12/DeWT_12 and log_2 DeL9_12/MoL9_12 as indicated) was confirmed by RT-qPCR. Values from biologically independent samples were normalized to the CBP20 internal control, and related to untreated (DEX-) plants, set to a value of 1. Data are mean ± SD analyzed by Mann-Whitney test; *, p <0.05. B) Relative expression of selected PTI/ETI-related genes based on the number of Fragments Per Kilobase of transcript sequence per Millions of base-pairs sequenced (FPKM) in each of the three independent samples per condition used for RNA-Seq. Actin expression is shown as control. Note that the expression levels of each individual replicate within the DEX-treated BIR1 L9_12 group mirror the abundance of BIR1 transcripts in each replicate. Significant differences between mock-treated and DEX-treated samples were analyzed using two-way ANOVA followed by Sidak´s multiple comparison test; ****, adjusted p-value < 0.0001, *** < 0.001, **< 0.01. WT, wild-type Col-0; L9, BIR1 L9 transgenics; _4d, 4 days of treatment; _12d, 12 days of treatment. C) Western blot analysis of SUPPRESSOR OF BIR1-1 (SOBIR1) and PATHOGENESIS RELATED 1 (PR1) using specific antibodies in two independent sets of BIR1 L9 samples. Plants were mock-treated (-) or DEX-treated (+) for 12 days. The presence (+) or absence (-) of morphological phenotypes (Ph) in each sample is indicated. Protein loading control by Ponceau S is shown.

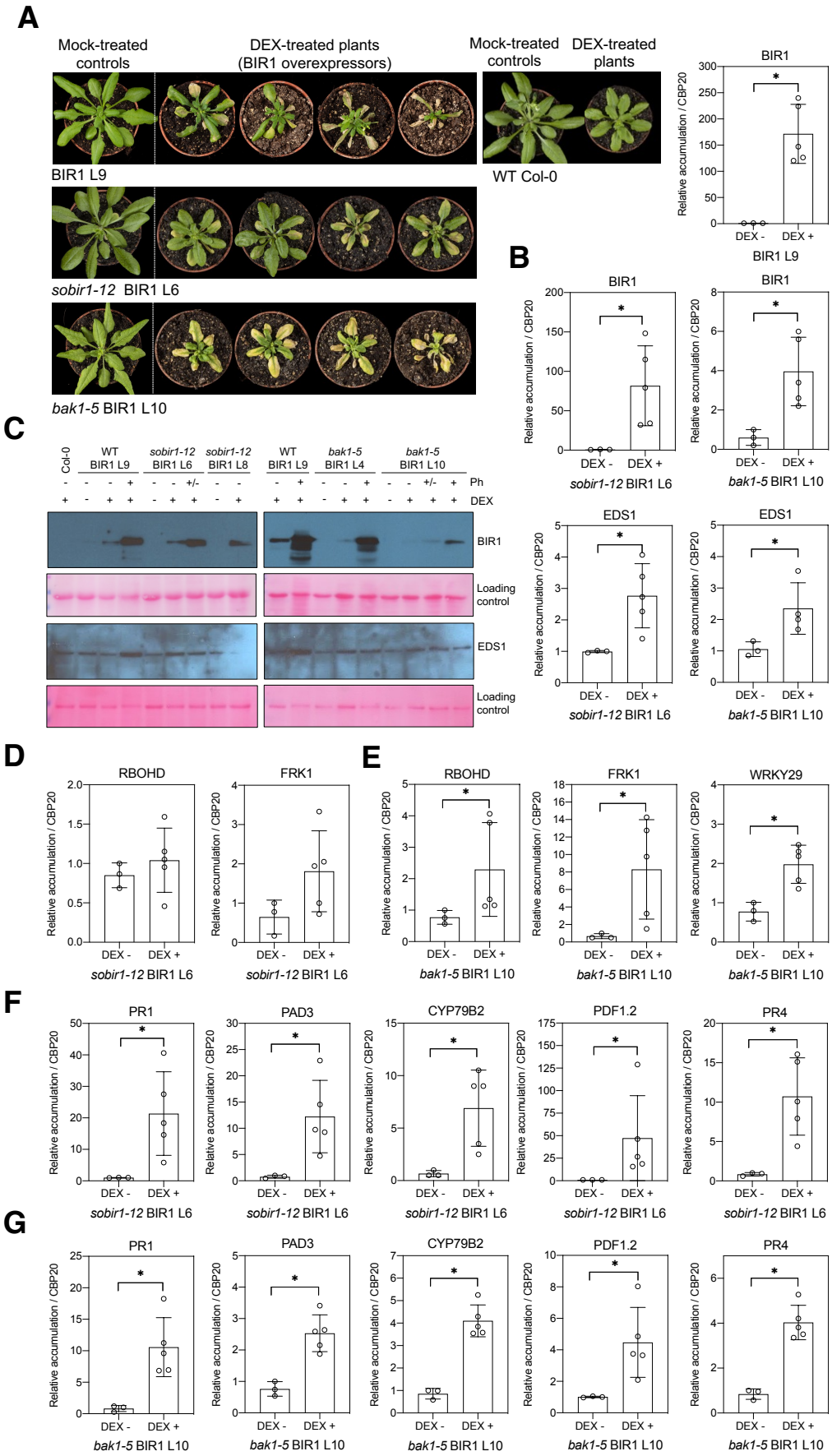
A
Mock-treated controls
DEX-treated plants (BIR1 overexpressors)
Mock-treated controls
DEX-treated plants
BIR1 L9
WT Col-0
sobir1-12 BIR1 L6
bak1-5 BIR1 L10
BIR1
Relative accumulation / CBP20
DEX -
DEX +
B
C
Col-0
WT BIR1 L9
sobir1-12 BIR1 L6
sobir1-12 BIR1 L8
WT BIR1 L9
bak1-5 BIR1 L4
bak1-5 BIR1 L10
Ph
DEX
BIR1
Loading control
EDS1
Loading control
EDS1
D
RBOHD
FRK1
E
RBOHD
FRK1
WRKY29
F
PR1
PAD3
CYP79B2
PDF1.2
PR4
G

Figure 5. Phenotypes caused by BAK1-INTERACTING RECEPTOR-LIKE KINASE 1 (BIR1) overexpression are partially rescued in *sobir1-12* mutants, but not in a *bak1-5* mutant.

A) Morphology of transgenic *sobir1-12* BIR1 L6 and *bak1*-5 BIR1 L10 mutant plants expressing BIR1 under the control of a dexamethasone (DEX)-inducible 35S promoter. Transgenic BIR1 L9 plants in the wild-type (WT) Col-0 background are shown as a reference. Plants were grown for three weeks on soil and treated with 30 μM dexamethasone (DEX) to induce BIR1 transcription or mock-treated with H_2O. Non-transgenic WT Col-0 plants are shown as controls. Plants were photographed after 12 days of the first DEX/ H_2O application. Images from independent transgenic lines are shown in Fig. S7. RT-qPCR analysis of *BIR1* transcripts in BIR1 L9 plants are shown. B) RT-qPCR analysis of BIR1 and ENHANCED DISEASE SUSCEPTIBILITY 1 (EDS1) transcripts in *sobir1-12* BIR1 L6 and *bak1*-5 BIR1 L10 plants. C) Western blot analysis of BIR1 and EDS1 proteins with specific antibodies in WT BIR1 L9 and two independent lines of *sobir1-12* BIR1 (L6, L8) and *bak1*-5 BIR1 (L4, L10). Plants were mock-treated (-) or DEX-treated (+) for 12 days as indicated. The presence (+) or absence (-) of morphological phenotypes (Ph) in each sample is indicated. Protein loading control by Ponceau S is shown. RT-qPCR analysis of the PTI-marker genes RESPIRATORY BURST OXIDASE HOMOLOG PROTEIN D (RBOHD), FLG22-INDUCED RECEPTOR-LIKE KINASE 1 (FRK1) or WRKY DNA-BINDING PROTEIN 29 (WRKY29) in *sobir1-12* BIR1 L6 (D) and *bak1*-5 BIR1 L10 (E) plants. RT-qPCR analysis of representative marker genes of the salicylic acid PATHOGENESIS RELATED 1 (PR1), jasmonic acid PLANT DEFENSIN 1.2 (PDF1.2), ethylene PR4 and camalexin [PHYTOALEXIN DEFICIENT 3 (PAD3), CYTOCHROME P450 MONOOXYGENASE 79B2 (CYP79B2)] pathways in *sobir1-12* BIR1 L6 (F) and *bak1*-5 BIR1 L10 (G) plants. In all cases, the same set of replicates from each genotype was used to measure all the genes shown in the graphs. Transcript accumulation was determined in mock-treated (DEX-) versus DEX-treated (DEX+) after 12 days of treatment. Values from biologically independent samples were normalized to the CBP20 internal control, and related to mock-treated plants, set to a value of 1. Data are mean ± SD analyzed by Mann-Whitney test; *, $p < 0.05$. Experiments were repeated at least twice with similar results.

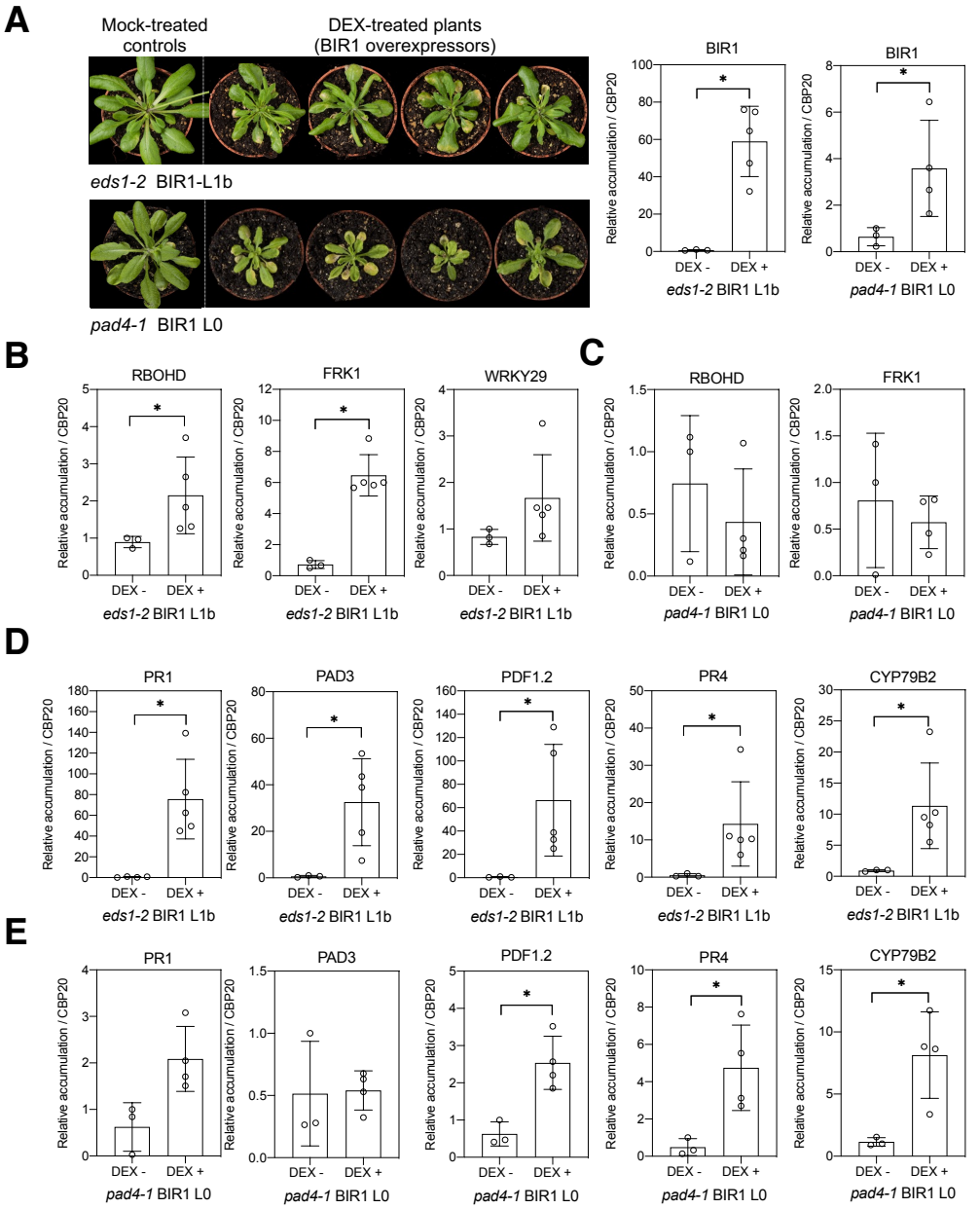

Figure 6. Phenotypes caused by BAK1-INTERACTING RECEPTOR-LIKE KINASE 1 (BIR1) overexpression are partially rescued in *eds1-2* mutants, but not in a *pad4-1* mutant.

A) Morphology of transgenic *eds1-2* BIR1 L1b and *pad4-1* BIR1 L0 mutant plants expressing BIR1 under the control of a dexamethasone (DEX)-inducible 35S promoter. Plants were grown for three weeks on soil and treated with 30 µM DEX to induce BIR1 transcription or mock-treated with H_2O. Plants were photographed after 12 days of the first DEX/ H_2O application. Images from independent transgenic lines are shown in Fig. S7. RT-qPCR analysis of BIR1 transcript in *eds1-2* BIR1 L1b and *pad4-1* BIR1 L0 mutant lines are shown. RT-qPCR analysis of the PTI-marker genes RESPIRATORY BURST OXIDASE HOMOLOG PROTEIN D (RBOHD) and FLG22-INDUCED RECEPTOR-LIKE KINASE 1 (FRK1) in *eds1-2* BIR1 L1b (B) and *pad4-1* BIR1 L0 (C) plants. RT-qPCR analysis of representative marker genes of the salicylic acid PATHOGENESIS RELATED 1 (PR1), jasmonic acid PLANT DEFENSIN 1.2 (PDF1.2), ethylene PR4 and camalexin [PHYTOALEXIN DEFICIENT 3 (PAD3), CYTOCHROME P450 MONOOXYGENASE 79B2 (CYP79B2)] pathways in *eds1-2* BIR1 L1b (D) and *pad4-1* BIR1 L0 (E) plants. In all cases, the same set of replicates from each genotype was used to measure all the genes shown in the graphs. Transcript accumulation was determined in mock-treated (DEX-) versus DEX-treated (DEX+) after 12 days of treatment. Values from biologically independent samples were normalized to the CBP20 internal control, and related to mock-treated plants, set to a value of 1. Data are mean ± SD analyzed by Mann-Whitney test; *, $p < 0.05$. Experiments were repeated at least twice with similar results.

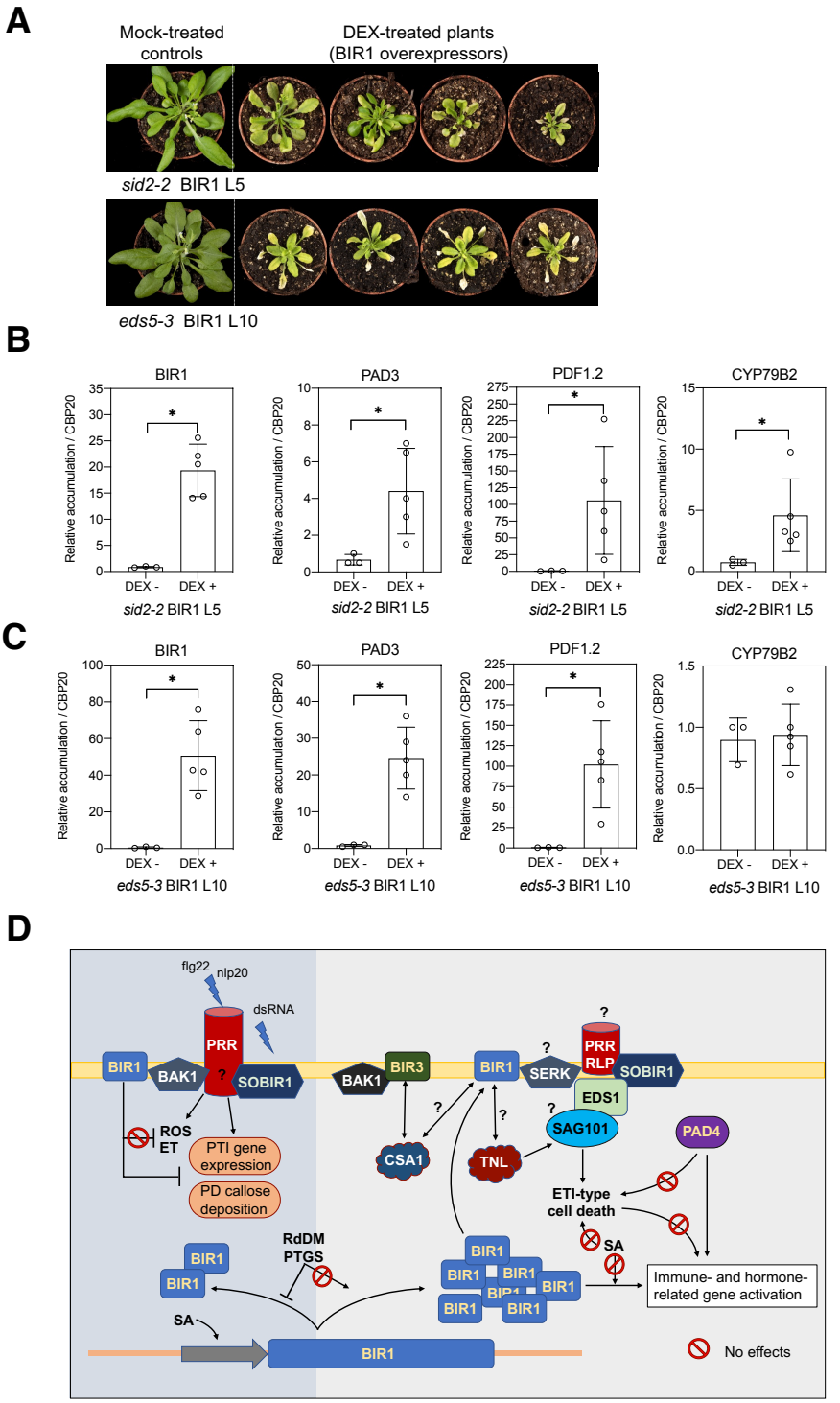

Figure 7. Phenotypes caused by BAK1-INTERACTING RECEPTOR-LIKE KINASE 1 (BIR1) overexpression are independent of salicylic acid (SA)-mediated signaling pathways.

A) Morphology of transgenic *sid2-2* BIR1 (L5) and *eds5-3* BIR1 (L10) mutant plants expressing BIR1 under the control of a dexamethasone (DEX)-inducible 35S promoter. Plants were grown for three weeks on soil and treated with 30 µM DEX to induce BIR1 transcription or mock-treated with H_2O. Plants were photographed after 12 days of the first DEX/ H_2O application. Images from independent transgenic lines are shown in Fig. S7a, b. RT-qPCR analysis of BIR1 and representative marker genes of the jasmonic acid PLANT DEFENSIN 1.2 (PDF1.2) and camalexin [PHYTOALEXIN DEFICIENT 3 (PAD3), CYTOCHROME P450 MONOOXYGENASE 79B2 (CYP79B2)] pathways in *sid2-2* BIR1 (L5) (B) and *eds5-3* BIR1 (L10) (C) mutant lines. In all cases, the same set of replicates from each genotype was used to measure all the genes shown in the graphs. Transcript accumulation was determined in mock-treated (DEX-) versus DEX-treated (DEX+) after 12 days of treatment. Values from biologically independent samples were normalized to the *CBP20* internal control, and related to mock-treated plants, set to a value of 1. Data are mean ± SD analyzed by Mann-Whitney test; *, $p < 0.05$. Experiments were repeated at least twice with similar results. D) Tentative working model for BIR1 homeostasis. SA-mediated transcription of BIR1 is regulated by RNA-directed DNA methylation (RdDM) and post-transcriptional RNA silencing (PTGS) (Guzman-Benito *et al.*, 2019). In these conditions, BIR1 induction interferes with PTI gene expression and PD callose deposition triggered by various elicitors (flg22, nlp20, dsRNA). Loss of BIR1 regulation leads to constitutive BIR1 induction and ultimately BIR1 overexpression at levels that cause SA-independent up-regulation of immune and hormone genes. BIR1 overexpression is sensed by one or several TNLs, of which CSA1 is a plausible candidate, to promote PAD4-independent ETI-type cell death that requires EDS1 and SOBIR1.

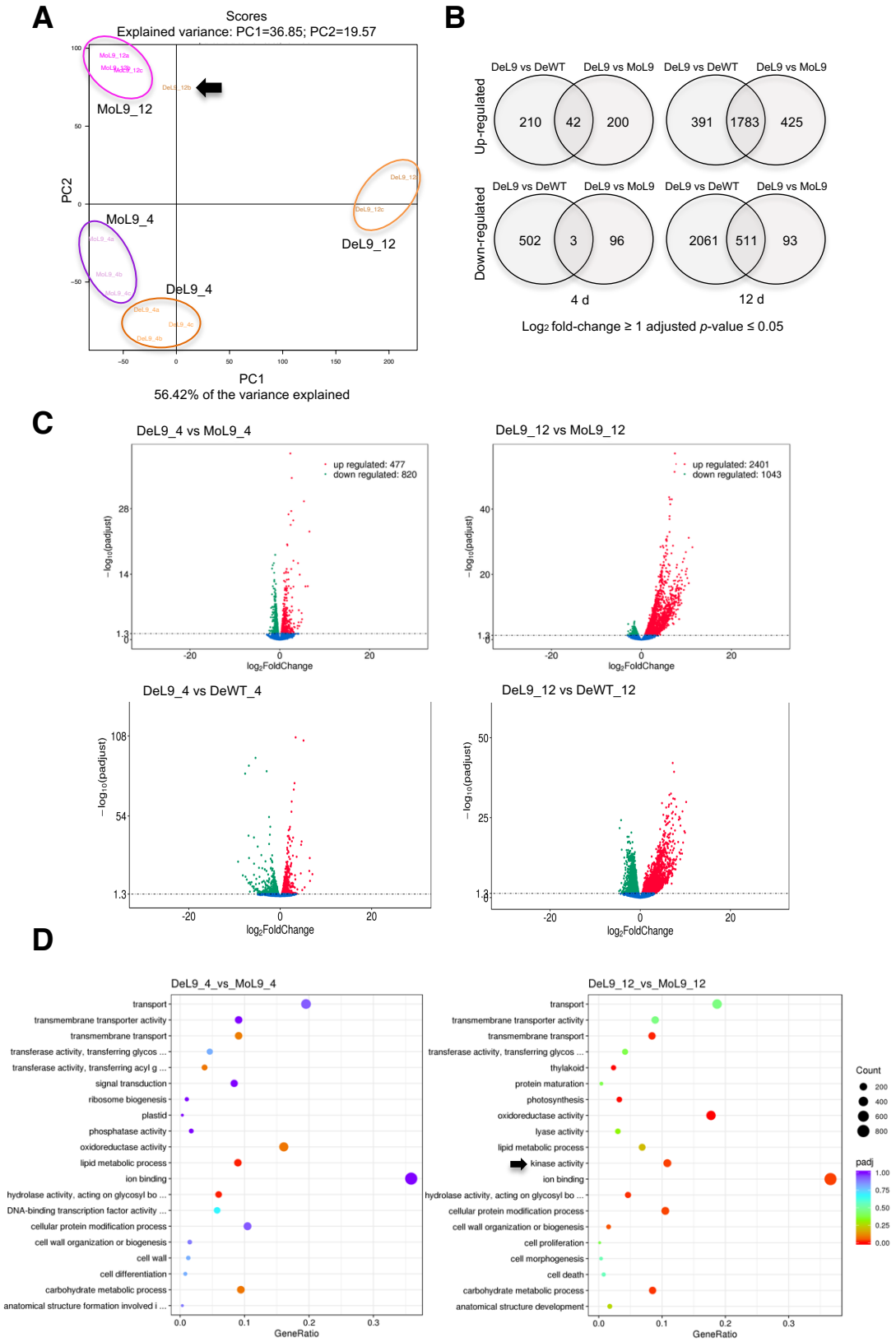

Figure S1. Transcriptomic profiling of BAK1-INTERACTING RECEPTOR-LIKE KINASE 1 (BIR1) expressing transgenic lines.
A) Principal component analysis (PCA) of RNA-Seq data. The PCA was performed using normalized RNA-Seq data of differentially expressed genes (DEGs) between dexamethasone (DEX)-treated and mock-treated transgenic BIR1 L9 plants after 4 and 12 days of treatment (DeL9_vs MoL9_). Each biological replicate is represented in the score plot. The variance explained by each component (%) is given in parentheses. B) Number of up-or down-regulated transcripts, with a $|\log_2$ (Fold-Change)$| \geq 1$ and adjusted p-value ≤ 0.05, in each pairwise comparison as indicated. C) Volcano plots showing the distribution of DEGs (adjusted p-value $\leq$ 0.05). The x-axis shows the fold change in gene expression between samples, and y-axis shows the statistical significance of the differences. Significantly up- and down-regulated genes are highlighted in red and green, respectively. Genes that are not differentially regulated are in blue. D) Scatterplot of selected gene ontology (GO) terms of DEGs. GO terms between wild-type (WT) and BIR1 L9 plants at 4 and 12 days after DEX-treatment (DeL9_ vs MoL9_) are shown. Dot size represents the count of different genes and the color indicates significance of the term enrichment. GO terms with adjusted p-value < 0.05 are significantly enriched. The kinase term (indicated by an arrow) was exclusively assigned to BIR1 L9 plants. WT, wild-type Col-0; L9, BIR1 L9 transgenic plants; De, DEX-treated plants; Mo, Mock-treated plants; _4, 4 days of treatment; _12, 12 days of treatment.

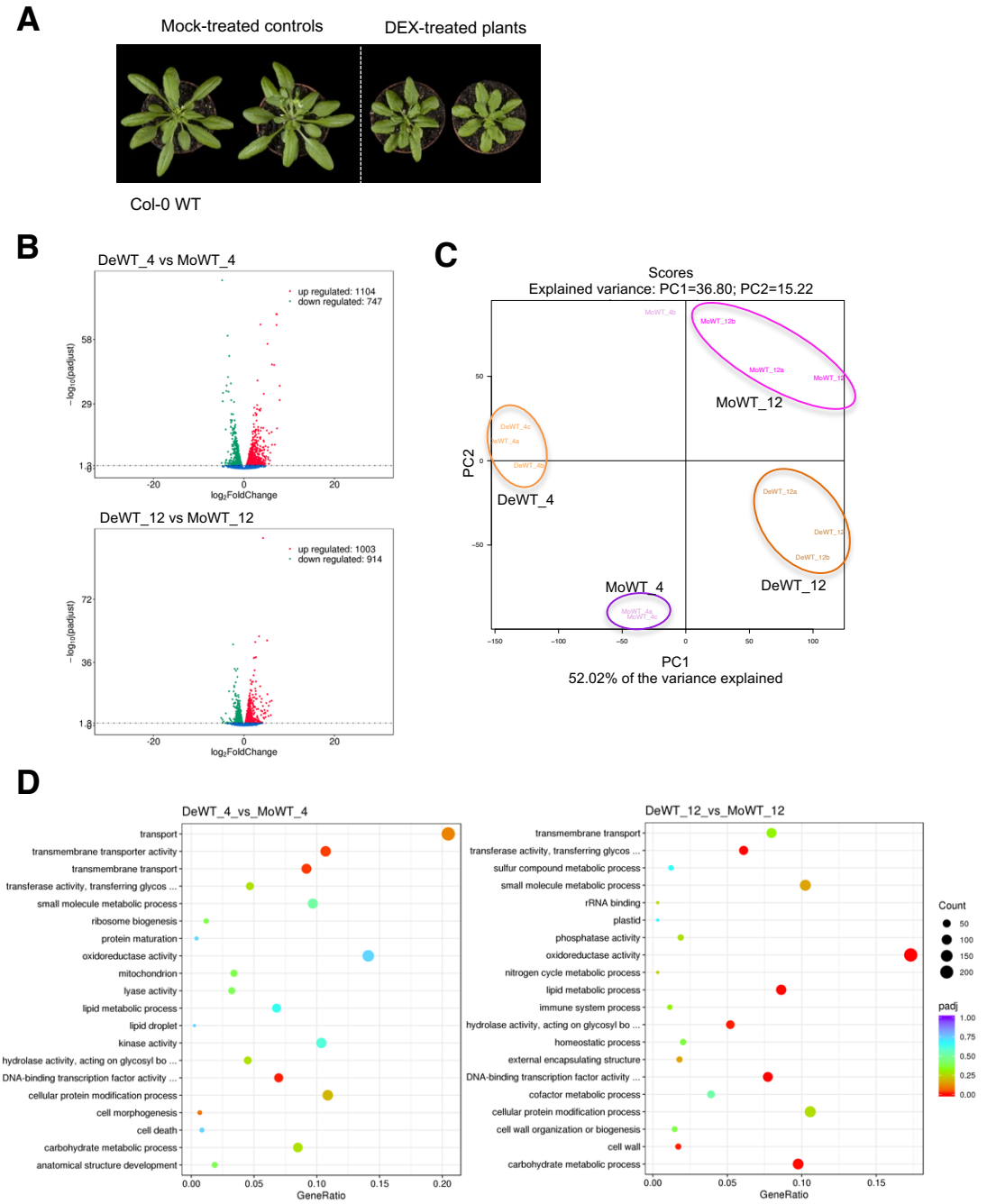

Figure S2. Transcriptomic profiling of dexamethasone (DEX)-treated wild-type Col-0 plants.
A) Morphology of representative wild-type (WT) Arabidopsis plants used for RNA-Seq experiments. Samples were collected after 4 or 12 days of 30 µM DEX treatment and subjected to RNA sequencing. H_2O-treated plants were used as controls. Note that application of DEX has a negative effect on plant growth as deduced by the significant reduction of rosette size after 12 days of DEX treatment relative to the non-treated controls. Box and whisker plot showing 5-95 percentile was analyzed by Mann-Whitney test; ****, p <0.0001. B) Volcano plots showing the distribution of differentially expressed genes (DEGs) (adjusted p-value ≤ 0.05). The x-axis shows the gene fold change, and y-axis plots the statistical significance (p-value) of the differences. Significantly up- and down-regulated genes are highlighted in red and green, respectively. Genes that are not differentially regulated are in blue. C) Principal component analysis (PCA) of RNA-Seq data. The PCA was performed using normalized RNA-Seq data of DEGs between DEX-treated and mock-treated WT plants after 4 and 12 days of treatment (DeWT_vs MoWT_). Each biological replicate is represented in the score plot. The variance explained by each component (%) is given in parentheses. D) Scatterplot of selected gene ontology (GO) terms of DEGs. GO terms between DEX-treated and mock-treated WT plants at 4 and 12 days of treatment (DeL9_ vs MoL9_) are shown. Dot size represents the count of different genes and the color indicates significance of the term enrichment. GO terms with adjusted p-value < 0.05 are significantly enriched. WT, wild-type Col-0; De, DEX-treated plants; Mo, Mock-treated plants; _4, 4 days of treatment; _12, 12 days of treatment.

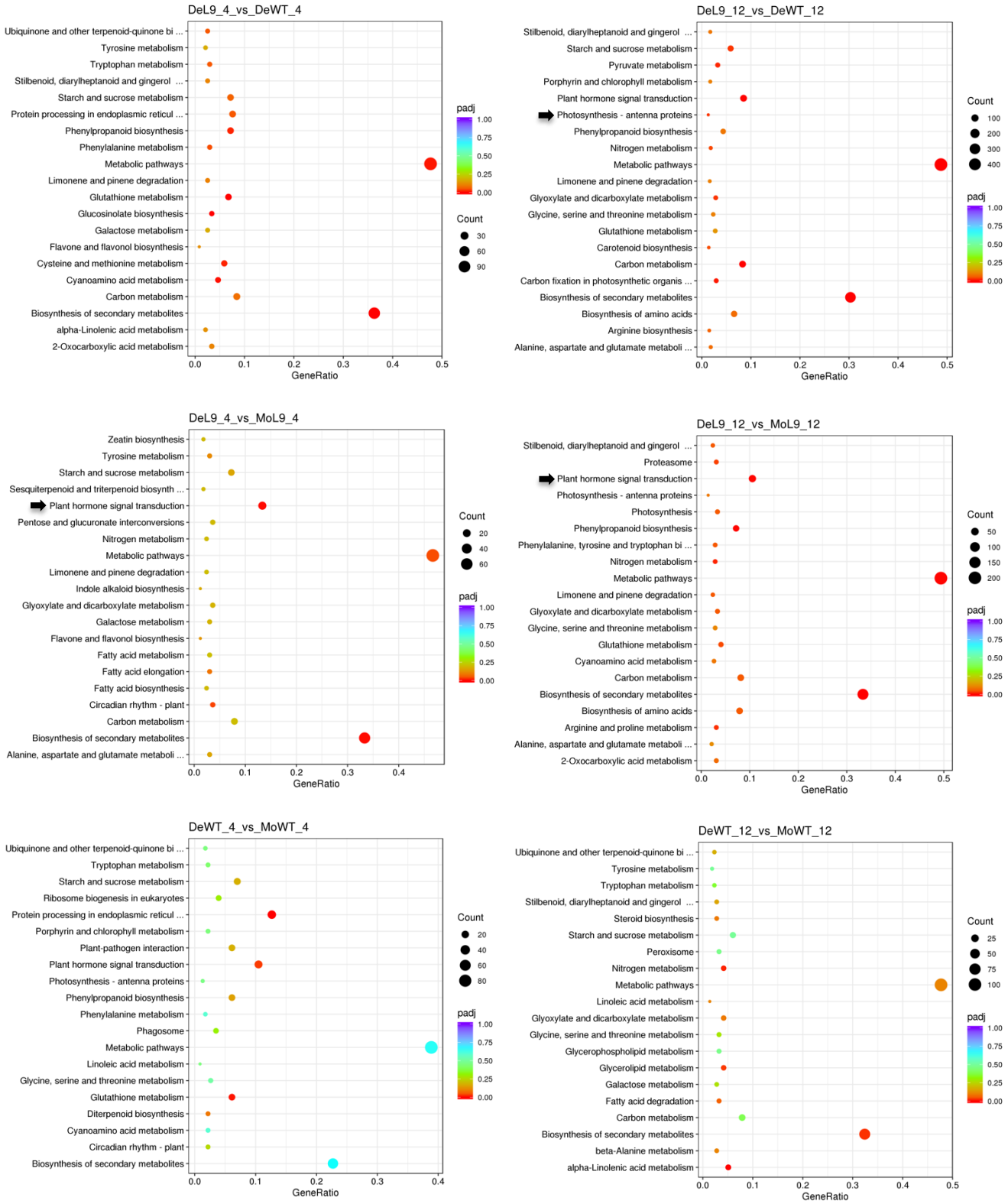

Figure S3. Enrichment analysis of Kyoto Encyclopedia of Genes and Genomes (KEGG) pathways using RNA-Seq data.
Scatterplot of selected Kyoto Encyclopedia of Genes and Genomes (KEGG) pathways. Dot size represents the count of different genes and the color indicates significance of the term enrichment. Terms with adjusted *p*-value < 0.05 are significantly enriched. WT, wild-type Col-0; De, DEX-treated plants; Mo, Mock-treated plants; _4, 4 days of treatment; _12, 12 days of treatment.

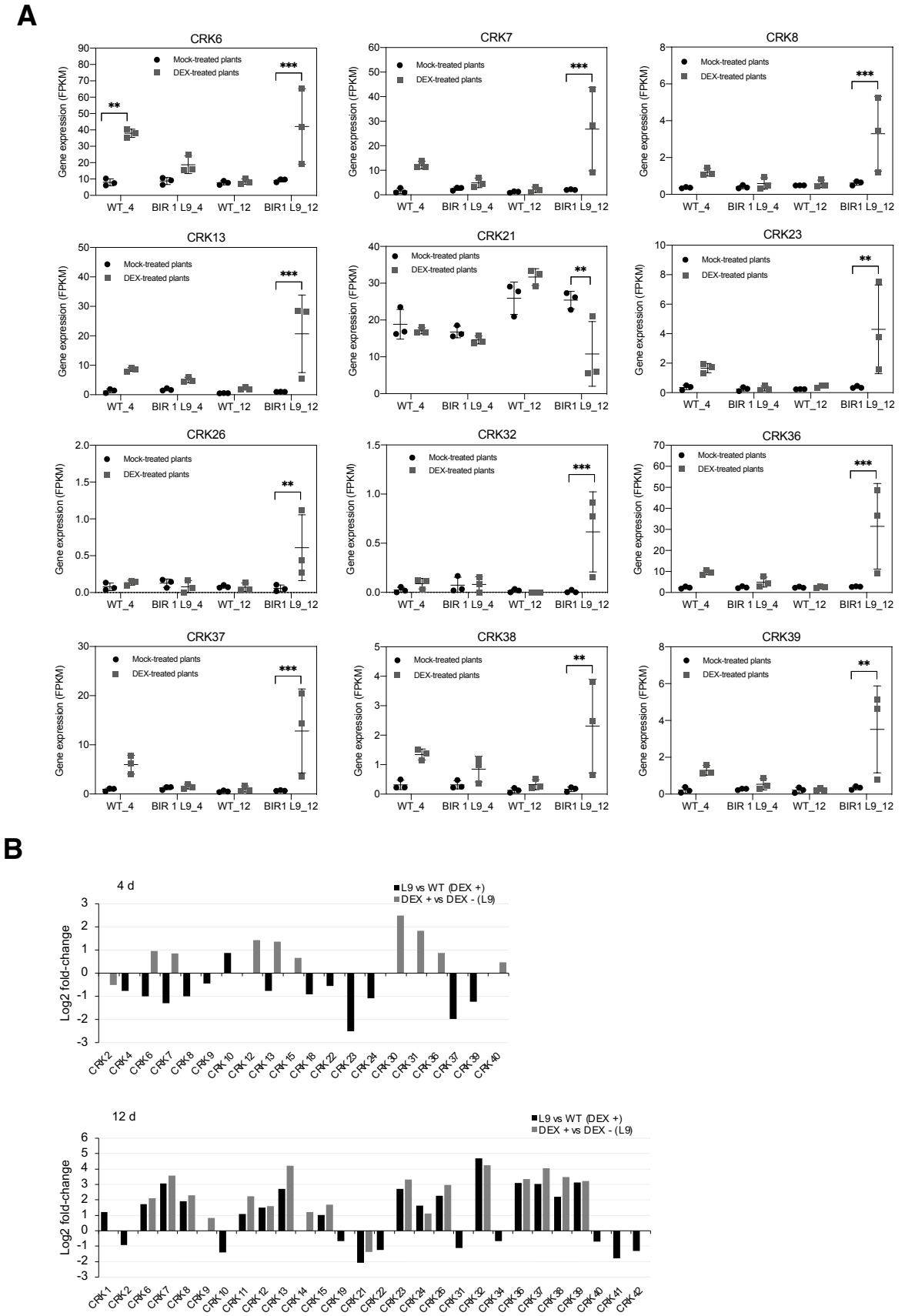

Figure S4. Differential expression of receptor-like protein (RLP)-coding genes in BAK1-INTERACTING RECEPTOR-LIKE KINASE 1 (BIR1) overexpressing plants.

A) Relative expression levels of selected RLP-coding genes based on the number of Fragments Per Kilobase of transcript sequence per Millions of base-pairs sequenced (FPKM) in each of the three independent samples per condition used for RNA-Seq. Significant differences between dexamethasone (DEX)- and mock-treated samples were analyzed using two-way ANOVA followed by Sidak´s multiple comparison test; ***, adjusted *p*-value < 0.001, **< 0.01. Note that the expression levels of each individual replicate within the DEX-treated BIR1 L9_12 group mirror the abundance of BIR1 transcripts in each replicate. B) Differential expression of selected BIR1-responsive RLP-coding genes based on $\log_2$ fold-change in the indicated pairwise comparisons. WT, wild-type Col-0; L9, BIR1 L9 transgenics; De, DEX-treated plants; Mo, mock-treated plants: _4d, 4 days of treatment; _12d, 12 days of treatment.

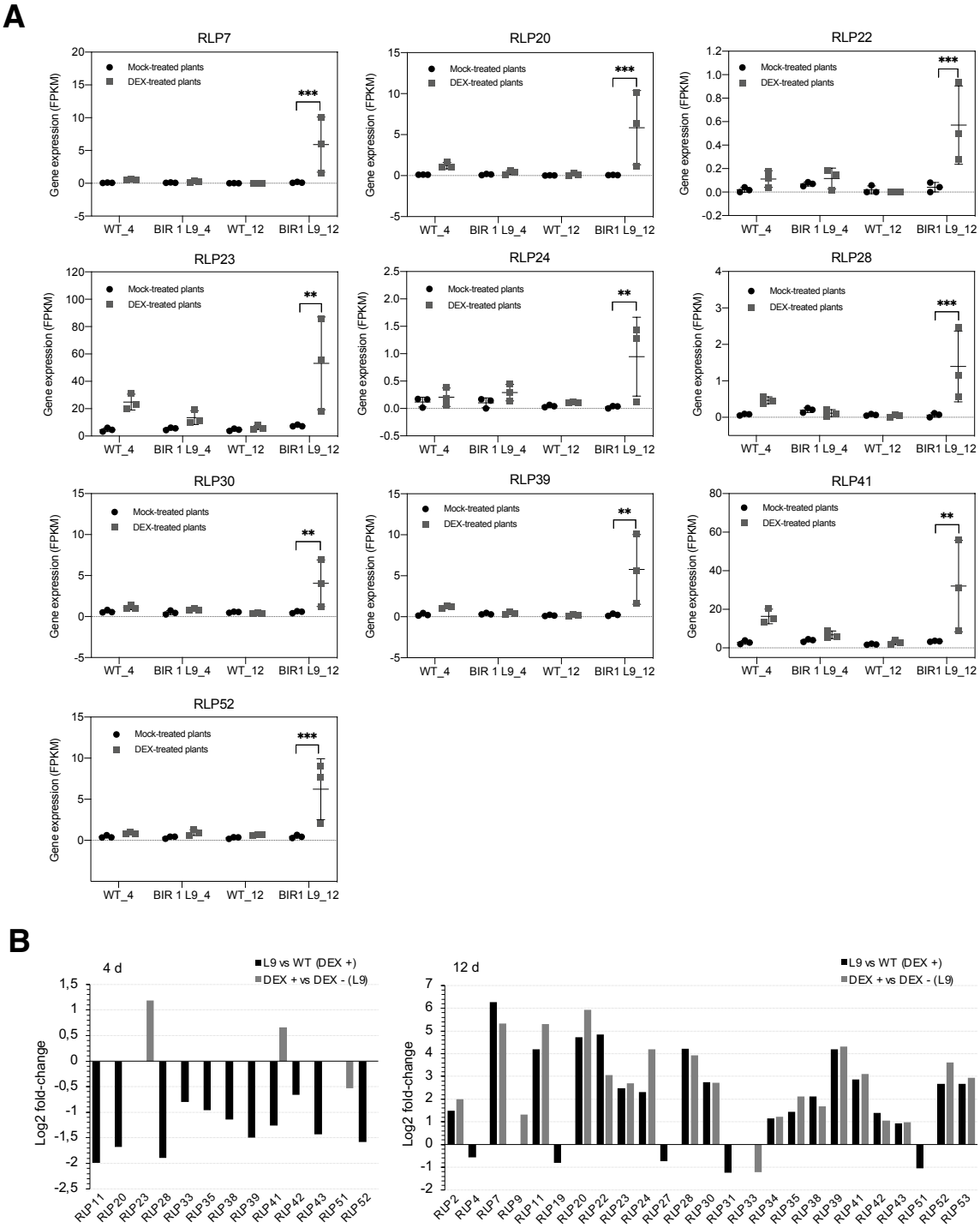

Figure S5. Differential expression of cysteine-rich receptor-like kinase (CRK)-coding genes in BAK1-INTERACTING RECEPTOR-LIKE KINASE 1 (BIR1) overexpressing plants.

A) Relative expression levels of selected CRK-coding genes based on the number of Fragments Per Kilobase of transcript sequence per Millions of base-pairs sequenced (FPKM) in each of the three independent samples per condition used for RNA-Seq. Significant differences between dexamethasone (DEX)- and mock-treated samples were analyzed using two-way ANOVA followed by Sidak´s multiple comparison test; ***, adjusted *p*-value < 0.001, **< 0.01. Note that the expression levels of each individual replicate within the DEX-treated BIR1 L9_12 group mirror the abundance of BIR1 transcripts in each replicate. B) Differential expression of selected BIR1-responsive CRK-coding genes based on log_2 fold-change in the indicated pairwise comparisons. WT, wild-type Col-0; L9, BIR1 L9 transgenics; De, DEX-treated plants; Mo, mock-treated plants: _4d, 4 days of treatment; _12d, 12 days of treatment.

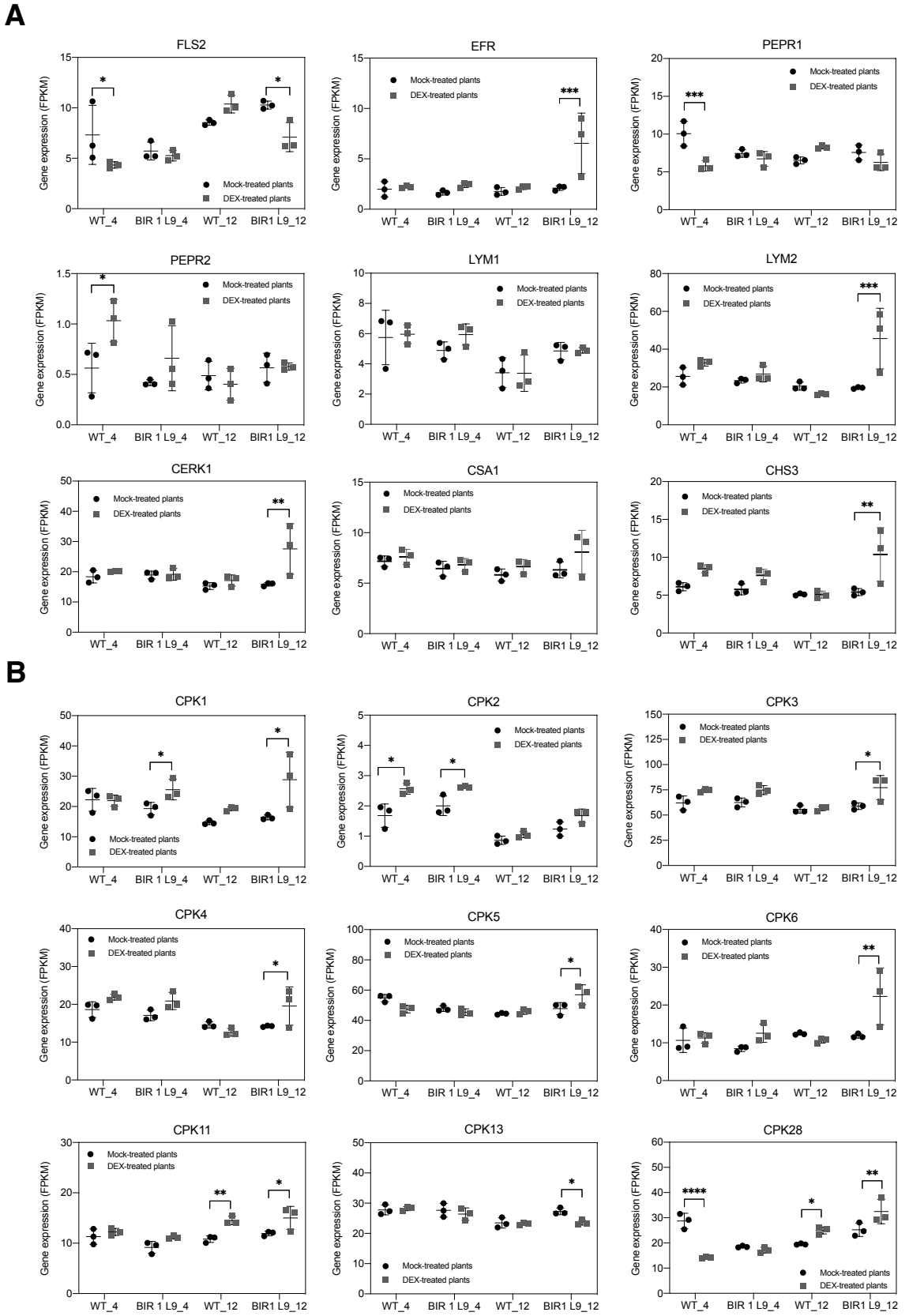

Figure S6. Differential expression of cell-surface pattern recognition receptors (PRR) and calcium-dependent protein kinases (CPK)-encoding genes in BAK1-INTERACTING RECEPTOR-LIKE KINASE 1 (BIR1) overexpressing plants.

Relative expression levels of selected PRR- (A) and CPK-coding genes (B) based on the number of Fragments Per Kilobase of transcript sequence per Millions of base-pairs sequenced (FPKM) in each of the three independent samples per condition used for RNA-Seq. Significant differences between dexamethasone (DEX)- and mock-treated samples were analyzed using two-way ANOVA followed by Sidak´s multiple comparison test; ***, adjusted *p*-value < 0.001, **< 0.01, *< 0.05. WT, wild-type Col-0; L9, BIR1 L9 transgenics; De, DEX-treated plants; Mo, mock-treated plants: _4d, 4 days of treatment; _12d, 12 days of treatment.

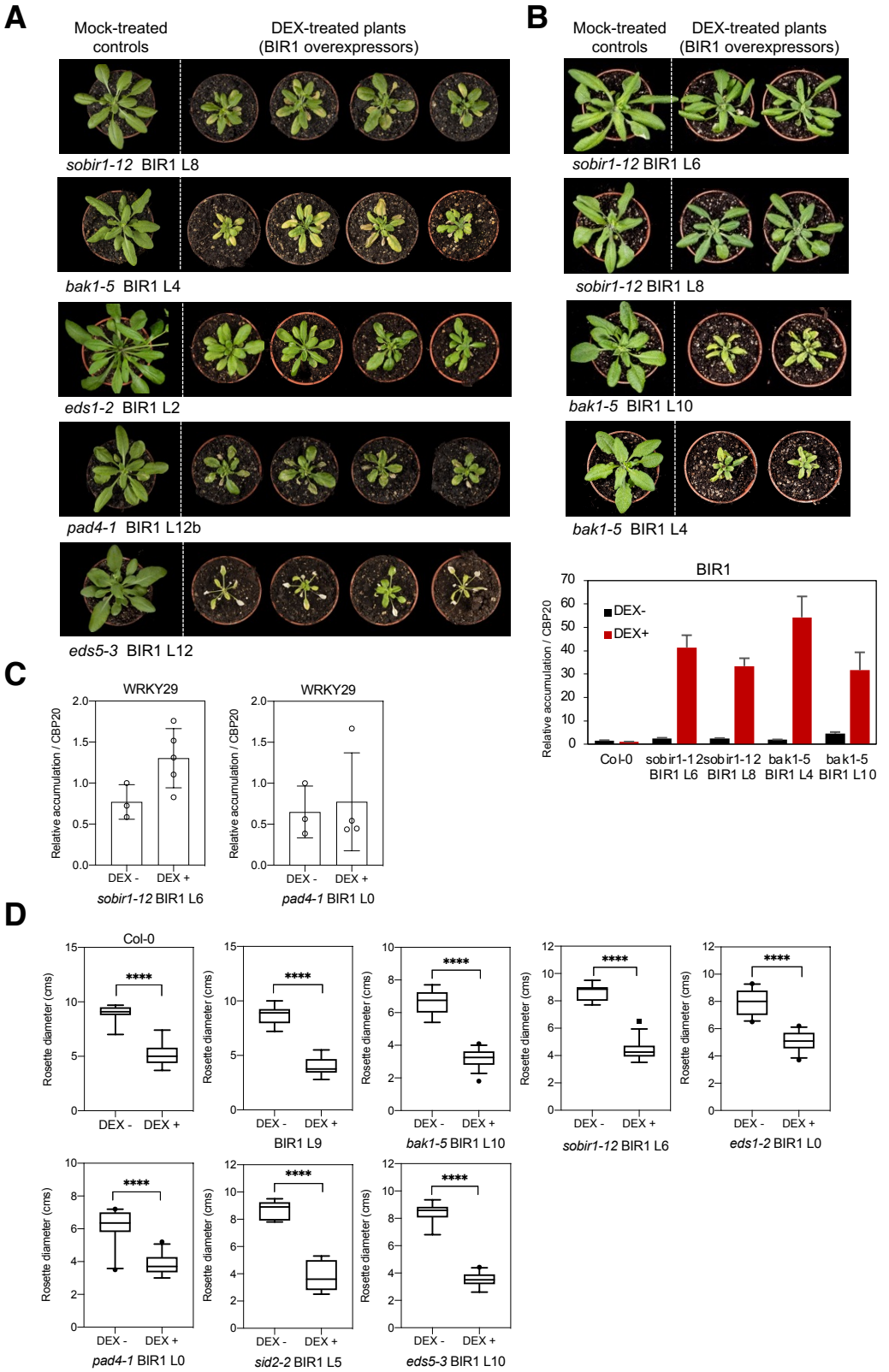

Figure S7. Morphological and growth defects in BAK1-INTERACTING RECEPTOR-LIKE KINASE 1 (BIR1) overexpressing plants of different immune mutant genetic backgrounds.

A) Morphology of transgenic *sobir1-12* BIR1 L8, *bak1-5* BIR1 L4, *eds1*-2 BIR1 L2, *pad4-1* BIR1 L12b and *eds5-3* BIR1 L12 mutant plants from independent lines expressing BIR1 under the control of a dexamethasone (DEX)-inducible 35S promoter. Plants were grown for three weeks on soil and treated with 30 µM DEX to activate BIR1 transcription or mock-treated with H_2O. Plants were photographed after 12 days of the first DEX/ H_2O application. B) Morphology and BIR1 expression levels of DEX- and mock-treated *sobir1-12* BIR1 (L6, L8) and *bak1-5* BIR1 (L4, L10) plants as observed in different biological replicates of the experiment. qRT-PCR analysis showed comparable BIR1 transcript levels in both genotypes. Each sample consisted of RNA pooled from six different plants. C) RT-qPCR analysis of the PTI-marker WRKY DNA-BINDING PROTEIN 29 (WRKY29) gene in *sobir1-12* BIR1 L6 and *pad4*-1 BIR1 L10 mutant backgrounds. In all cases, transcript accumulation was determined in DEX-treated (DEX+) versus mock-treated (DEX-) after 12 days of treatment. Values from biologically independent samples were normalized to the CBP20 internal control, and related to mock-treated plants, set to a value of 1. Data are mean ± SD analyzed by Mann-Whitney test; *, $p < 0.05$. D) Rosette size (diameter) in wild-type (WT) and BIR1 overexpressing ETI/PTI mutants after 12 days of DEX treatment relative to the non-treated controls. Box and whisker plots showing 5-95 percentile were analyzed by Mann-Whitney test; ****, $p < 0.0001$. Note that rosette size is largely influenced by the effect of DEX on plant development as shown for WT Col-0 plant in this study.